UPPSALA
UNIVERSITET

ISRN UTH-INGUTB-EX-E-2011/10-SE
Examensarbete 15 hp
November 2011

Measurement setup for High Power Impulse Magnetron Sputtering

Ólafur Björgvin Sveinsson

UPPSALA
UNIVERSITET

Teknisk- naturvetenskaplig fakultet
UTH-enheten

Besöksadress:
Ångströmlaboratoriet
Lägerhyddsvägen 1
Hus 4, Plan 0

Postadress:
Box 536
751 21 Uppsala

Telefon:
018 – 471 30 03

Telefax:
018 – 471 30 00

Hemsida:
http://www.teknat.uu.se/student

Abstract

Measurement setup for High Power Impulse Magnetron Sputtering

Ólafur Björgvin Sveinsson

Recently material physics group at Science Institute of University of Iceland has been using reactive sputtering to grow thin films used in various research projects at the institute. These films have been grown using dc sputtering which has been proven a very successful method. High power impulse magnetron sputtering or HiPIMS is an new pulsed power sputtering method where shorter but high power pulses are used to sputter over lower steady power. The project resulted in a functional system capable of growing thin films using HiPIMS. Thin films grown with high power pulses have a higher film density and other more preferable properties compared to films grown using direct current magnetron sputtering.

Handledare: Sveinn Ólafsson
Ämnesgranskare: Lars Ericsson
Examinator: Nóra Masszi
ISRN UTH-INGUTB-EX-E-2011/10-SE

Sammanfattning

The Science Institute of the University of Iceland har dom senaste åren använt tunna filmer i flera projekt hos institutet till exempel för att hitta ett lämpligt ämne att förvara väte i för framtidens vätefordon. Dessa filmer är producerade på plats i en av institutets ”sputtering chambers”, genom åren har en sputtering metod kallad direct current Magnetron Sputtering använts för att göra filmer. Men nyligen har institutetet köpt ett nytt nätaggregat som gör det möjligt att göra filmer med en ny metod kallad High Power Impulse Magnetron Sputtering. För att kunna använda nya metoden måste några ändringar tillföras till det befintliga systemet. Projektets mål var att implementera hårdvara/mjukvara så att institutet kan producera filmer och studera filmer skapade med den nya metoden.

Projektet har resulterat i ett system som i dag används för produktion av tunna filmer med High Power Impulse Magnetron Sputtering metoden. Metoden har visat sig skapa tunna filmer som är tätare och slätare än filmer gjorda med direct current Magnetron Sputtering. Dessutom har projektet resulterat i två vetenskapliga artiklar publicerade i Journal of Applied Physics och Thin Solid Films om High Power Impulse Magnetron Sputtering.

Summary

The purpose of this project was to design and test a measurement system for high power impulse magnetron sputtering. High powered impulse magnetron sputtering or HiPIMS is a new pulsed power sputtering method.

The system is used to study the different properties of thin films grown with HiPIMS by a research group in material physics at the University of Iceland.

Results from films grown with the system have shown that thin films grown using HiPIMS lead to significantly smoother films and produces highly crystalline films even at room temperature whereas direct current Magnetron Sputtering or dcMS resulted in films with larger crystallites embedded in amorphous matrix. Furthermore the reactive HiPIMS discharge differs significantly from non-reactive in a somewhat counter intuitive fashion.

Abbrevations

dcMS - direct current Magnetron Sputtering
HiPIMS – High Power Impulse Magnetron Sputtering
DAQ – Data AcQuisition

Foreword

This report is a part of an examination project for a Bachelor degree in Electrical Engineering at Uppsala University.

Lately the material physics group at the Science Institute of Iceland has been using reactive sputtering to grow thin films used in various research projects at the institute. These films have been grown using direct current magnetron sputtering which has been proven a very successful method. Recently the group acquired a power supply making HiPIMS an option to grow thin films. The research institute is therefore in need of hardware and software development.

Table of Contents

1. Introduction

The goal of this project is to design and test a system capable of growing thin films using high impulse magnetron sputtering (HiPIMS) and if time allows study the properties of thin films grown using HiPIMS vs direct current magnetron sputtering (dcMS).

The research group at the Science Institute of Iceland has two sputtering systems, Dracula and Spike (figure 1 and 2). Both systems currently grow thin films using dcMS.

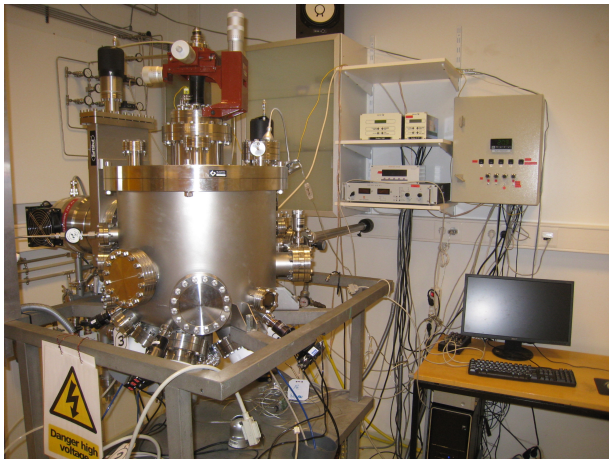

Figure 1: Dracula.

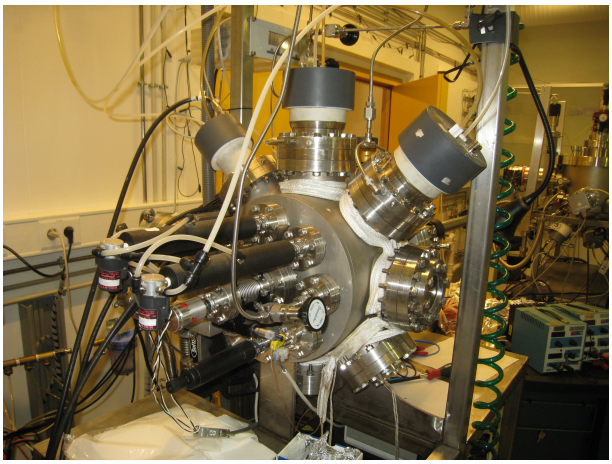

Figure 2: Spike.

These systems consist of a sputtering chamber with pressure/temperature meters, magnetron shutters controlled by a PC, manually controlled gas valves and heater for the baking process. Dracula and Spike have mostly the same equipment. The main difference being that Spike is equipped to measure sample resistance during growth but only has three magnetrons while Dracula cannot measure resistance during growth but has five magnetrons.

Figure 3: Power supply and pulser with power monitor box and Agilent 5462A oscilloscope on top of it.

A new power supply has recently been acquired which consists of a Maris GS, 30 a 3kW 0-1000V DC supply and pulser with a 8F capacitor. The capacitor when fully loaded to 1000V has 4MJ energy stored. Maximum applied power to the magnetron is 600W(J/s) that energy hardly affects the capacitor during usage so the voltage is always steady. The power supply only has rudimentary internal pulse control but can be pulsed with an external signal. It also has a power monitoring unit which sends analog signals representing the voltage and current going through the system.

2. Problem description

Since the new power supply only has rudimentary pulse control and the power monitor unit sends analog signals the following problems have to be solved.

1. Implement hardware capable of sending trigger pulses (10us precision) to the power supply specified by the user.
2. Find a way to measure the power monitor signals (±10V and 1Msample/s or better), process and present the data gathered.
3. Design a program that can control the sputtering process and record the data from 1. and 2.

3. Theory

3.1 Sputtering and thin films

Thin films can be grown with different methods with thickness ranging from one nanometer to a few micrometers using magnetron sputtering. Magnetron sputtering is a technique where a thin film is grown on a substrate in a sputtering chamber. The sputtering chamber (see figure 4) is equipped with magnetrons, vacuum pumps, a heater, gas inlets and pressure/temperature meters.

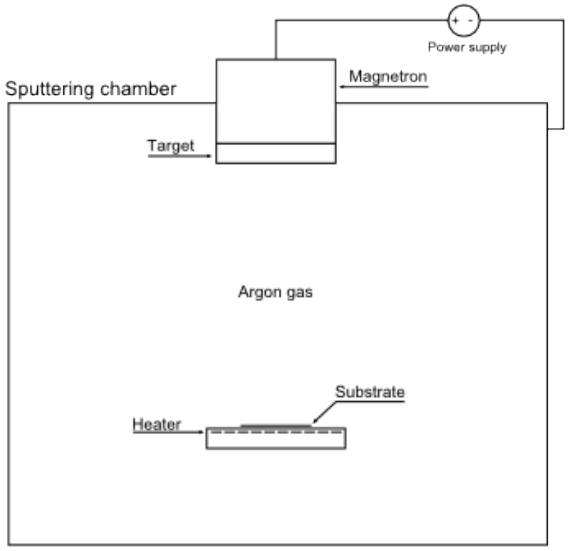

Figure 4: Sputtering chamber with one magnetron and heater.

A magnetron serves as an electrical connection to the target that is mounted on the magnetron. The target is a high purity (99.9% or purer) disk of some desired material which the film is sputtered from. Most system have multiple magnetrons making it possible to grow films made from different materials (Titanium film with platinum layers for example). A power supply is connected to the magnetron (cathode) and the chamber (anode), depending on what type of power supply is used it's either called dcMS (dc power supply) or HiPIMS (high power pulser).

Growth of thin films is done in two phases. The substrate goes through an annealing process, by pumping the chamber down to a pressure of 10^{-7} mbar and the substrate is heated to 500-600°C which removes oxygen and other impurities in the substrate. Then the chamber is filled with an inert gas (Argon most common) putting the pressure in the chamber at 10^{-3} mbar. In some cases an additional gas is added as a reactant. This type of sputtering is called reactive sputtering and used to make TiN, MgH_2 (nitrous gas or hydrogen gas added) for example. When the power is switched on the plasma ignites (ionized Ar^+) and the ions are attracted towards the target and collide with it

sputtering some of the targets atoms off (see figure 5). These atoms scatter away causing some to hit the substrate and over time build up a thin film. In the case of reactive sputtering the atoms react with the reactant before hitting the target. The magnetic field from the magnets in the magnetron trap the plasma near the magnetron which lowers the voltage and gas pressure required to get the sputtering process started[1].

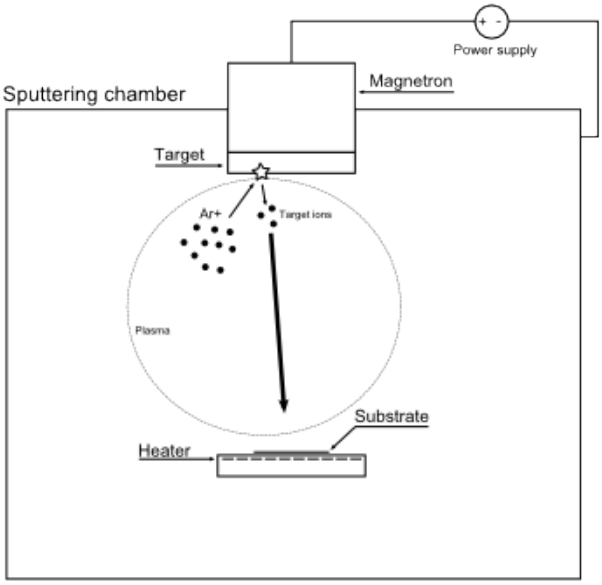

Figure 5: Growth process started, Ar ion collide with target causing some target atoms to be sputtered.

3.2 High Impulse Magnetron Sputtering

The main difference between dcMS and HiPIMS is that HiPIMS sends short and high voltage pulses while dcMS applies constant voltage. DcMS is limited to lower steady voltage to prevent arching and overloading the target/magnetron. Since HiPIMS uses short pulses (100-1000us) at 10-100Hz it can apply much higher voltage making the power during that time much higher than dcMS while the average power stays the same. The higher voltage sputters atoms from the target with higher energy making them more likely to be ionized. This leads to films being more dense and smoother when grown with HiPIMS compared to dcMS. Having ionized atoms also make it possible to put a voltage bias on the substrate accelerating sputtered atoms from the target to the sample to form even denser films. Thin films can be characterized by their different properties like thickness, density and roughness. These properties vary depending on what substrate or target is used, which sputtering technique and the sputtering systems parameters (gas pressure, temperature) during growth.

4. System design

4.1 Hardware

Two hardware solutions are needed:

- Hardware to send a signal to the supply
- Hardware to measure the power monitor.

Initial tries were done with a external waveform generator to send signals to the supply. This solution was discarded because changing the generators pulse waveform took too long. Instead a data acquisition (DAQ) card from National Instruments was acquired from an older system not in use. The DAQ card (NI PCI-6713) can send 1 Msample/s(1us pulses) and the waveform can be changed quickly (within 1 second).

To measure the power monitor two technical solutions were possible, using a DAQ card or a digital oscilloscope. The possibility to use a DAQ card was studied but the PCI-6713 is an analog output board and the computer did not have PCI slots available for another DAQ card. There are DAQ cards capable of doing both but because of limited funds one could not be purchased. Therefore a digital oscilloscope (Agilent 5462A 200 Msample/s) is used to measure the voltage and current in the process (figure 6 illustrates the equipment setup).

The digital oscilloscope has four inputs and the data is sent through a GPIB cable.

Four signals are measured during the process:

- control signal from the PC (used to trigger the oscilloscope and power supply)
- current and voltage from the power monitor
- ion current from the sample (only used when using Spike).

One problem with the oscilloscope is that it can only send data of three pulses every second while the pulses are sent at 10-100 Hz (pulses/s) which means not all pulses are logged. However, since there are limited funds for this project it will have to suffice. Nevertheless the data acquired is sufficient to analyze the growth process.

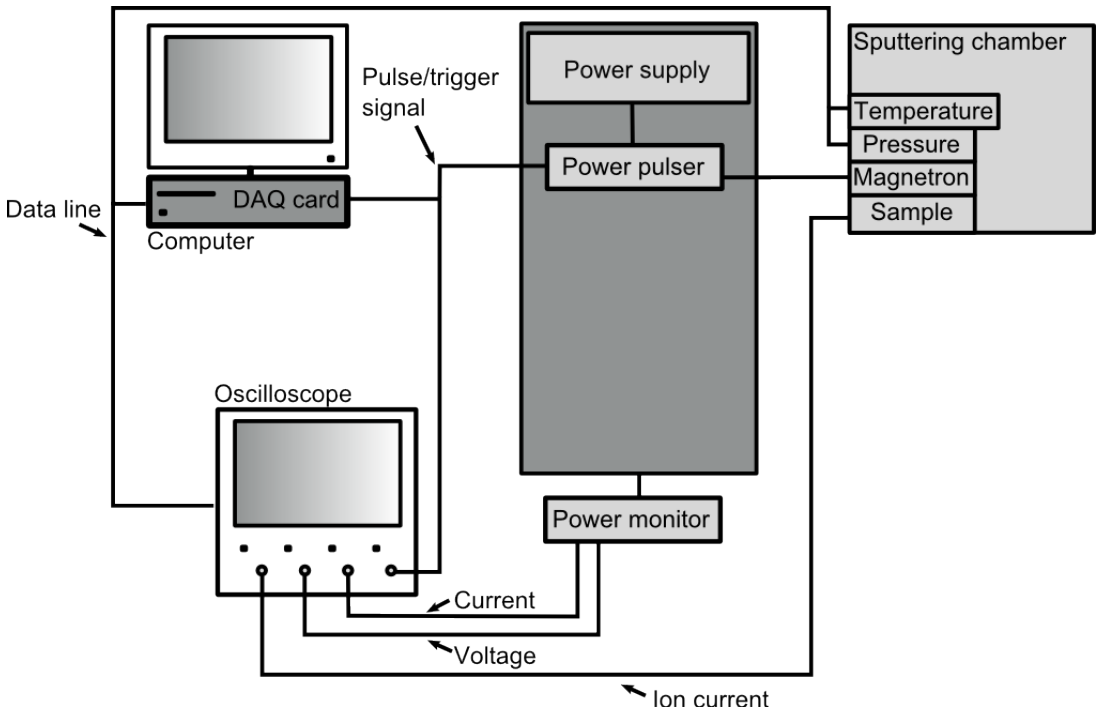

Figure 6: Layout of the measurement system.

4.2 Software

There are many software solutions to write a program that controls and gathers data from various instruments. The research group is currently using LabView programs making it the program of choice.

LabView is a graphical programming interface with graphical user interfaces for displaying data and controlling instruments. LabView is a powerful tool for making fast and simple programs capable of controlling and recording data from instruments. Most instruments include programs for LabView to control and get data from them.

The program has to meet the following design requirements.

1. It has to be able to log and display data from the power monitor.
2. Control the outgoing pulse to the power supply.
3. Include a data viewer capable of displaying multiple measurements.

4.3 LabView program: User Interface

LabView is divided into two parts when coding, the front panel and block diagram. The front panel contains the user interface where data from the executed code on the block diagram is displayed. Nodes are used to create programs in LabView and most objects on the front panel are also represented as nodes on the block diagram. These nodes are connected with wires which controls in what order the nodes are executed.

The user interface stands alone from the block diagram code. It is divided into two regions (as seen in figure 7), the gray region displays different pages depending on what tab is active. Each tab contains a small window with either controls or indicators relevant to the tab name. Latest measured values are shown in the blue area, this area is always visible independent of what tab pages is chosen. The upper right corner has three buttons that indicate if the data acquisition (oscilloscope) or pulse is on. The buttons can also be used to turn the data acquisition or pulse on or off and a third button is used to stop the program.

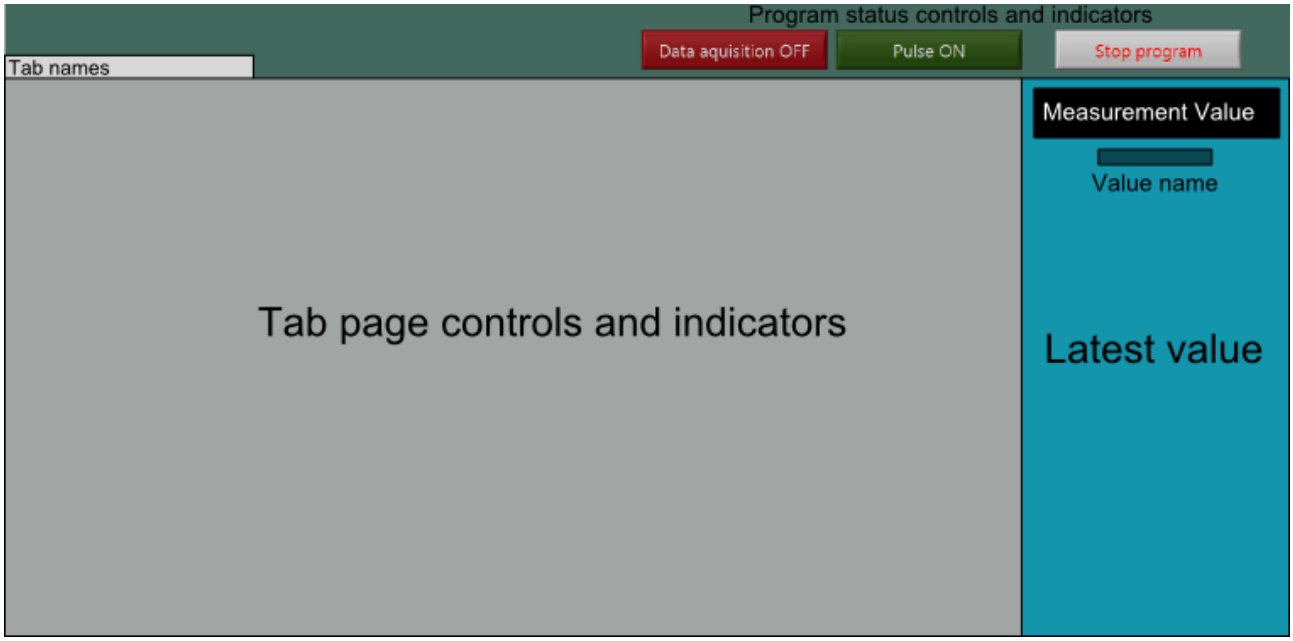

Figure 7: Shows the interface layout.

4.3.1 The control tab

The control tab (figure 8) interface contains controls to create the pulse sent by the DAQ card. User can pick the length, repeat frequency and if the pulse is negative or positive voltage. Repeat frequency can be changed at any time during growth, the DAQ card will update to the new frequency within a second. There are two graphs that show the outgoing pulse, the upper graph shows the pulse the DAQ card sends while the other graphs shows the signals measured by the oscilloscope. The graphs helps the user to see if changes to the pulse is needed to get the plasma stable, changing the pulse frequency and length of the pulse can help to get it stable.

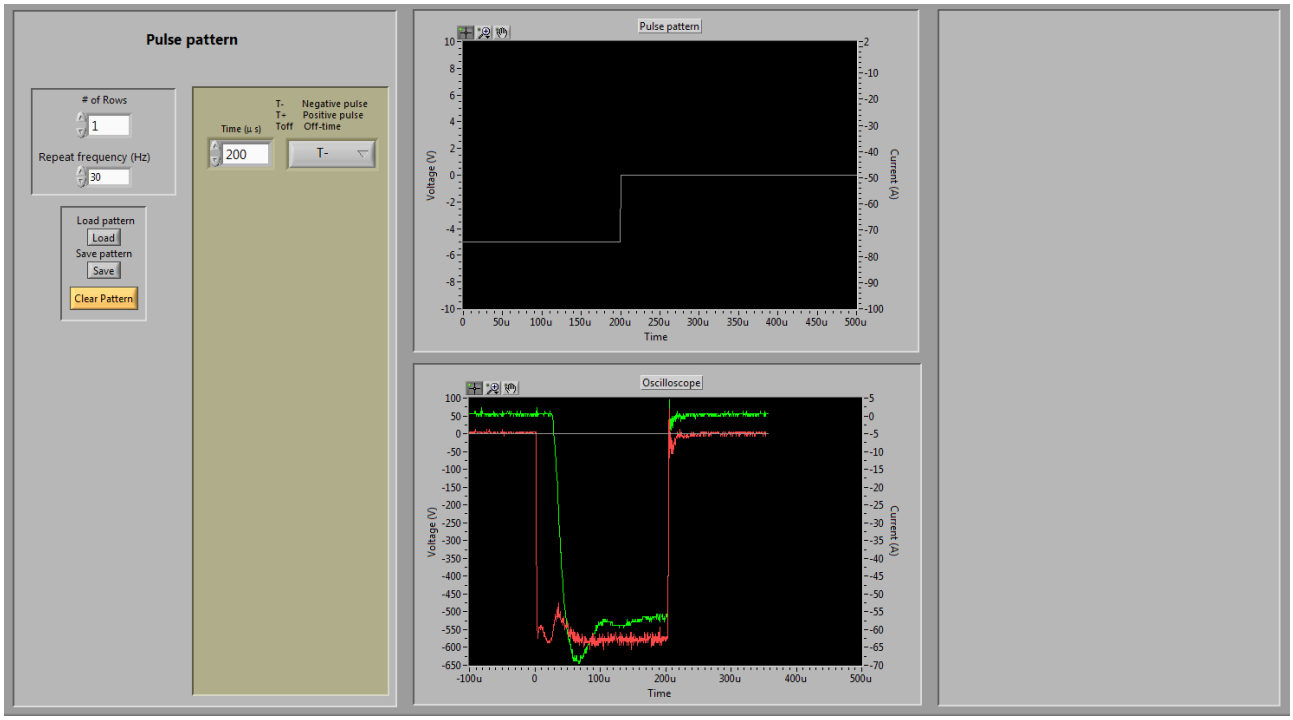

Figure 8: Control tab interface.

4.3.2 The measured data tab

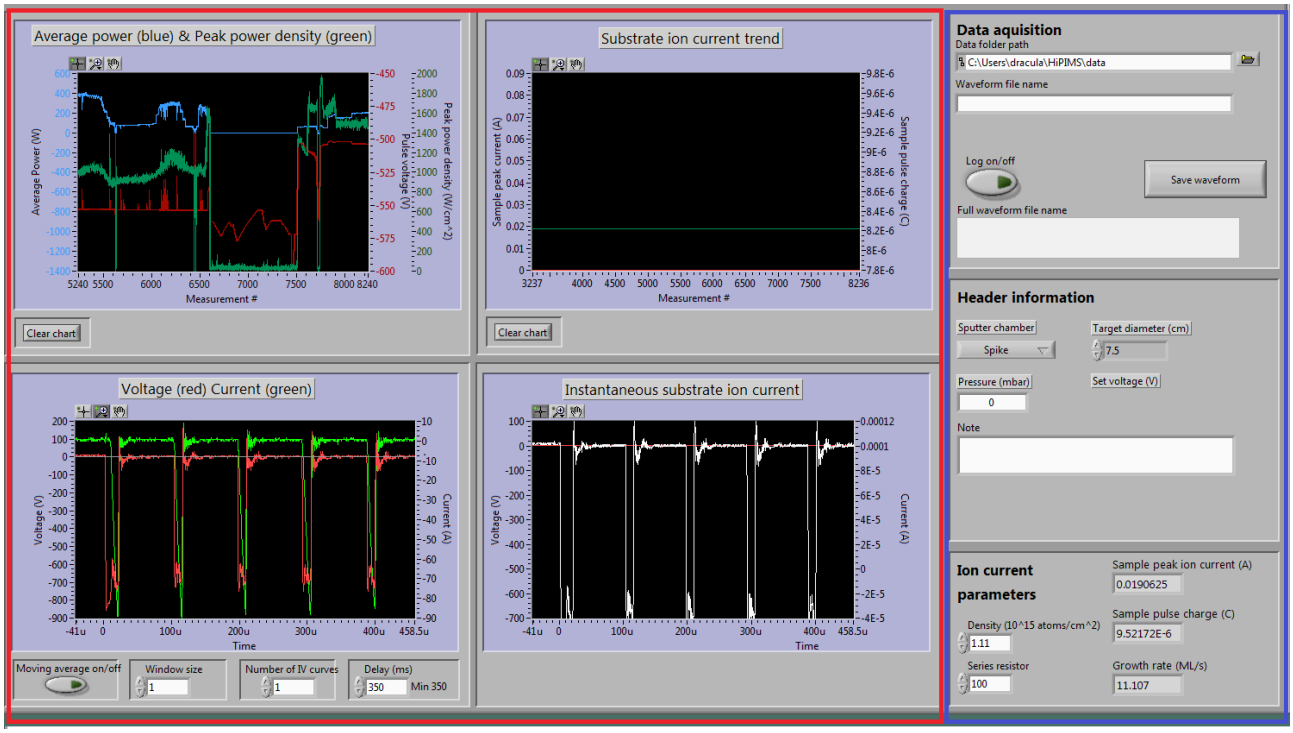

Figure 9: Data tab interface.

The data tab (figure 9) shows processed data and controls the log file and ion current settings. The interface is divided into two regions, red region presents data in four graphs and blue region has data log and ion current settings.

The four graphs in the red region show data processed from the oscilloscope. The lower left graph shows the raw data current/voltage from the power monitor and the upper left shows the history of three values (Average power, Peak power density and Pulse voltage). Other two graphs monitor substrate ion current which can only be measured in Spike. Substrate ion current is done by measuring the current going through the substrate during growth, it gives a good idea of how long the deposition of atoms lasts for each pulse and a rough estimate of growth rate.

In the bottom left corner there is an option to take a moving average of the data received to remove noise in the received signal (figure 10).

Figure 10: Moving average button and settings Window size decides number of samples averaged and Number of IV curves how many curves to average over. Delay(ms) is the sample delay of the oscilloscope.

The controls in the blue region(figure 9) control the path of the log file and waveform file. Data log is toggled on/off by the *Log on/off* button and will prompt for a new log file to be created or existing file path chosen when first pressed and then show the path chosen which can be changed at any time. The log file records the latest values seen on the right(figure 7). *Save waveform* button saves the latest pulse in a separate file.

4.3.3 Last saved file tab

The last saved file tab(figure 11) is a simple tab added so that the user can verify if the last saved waveform is acceptable. Waveforms measured vary during growth and once in a while you get some that are ruined by noise that the user does not want to save.

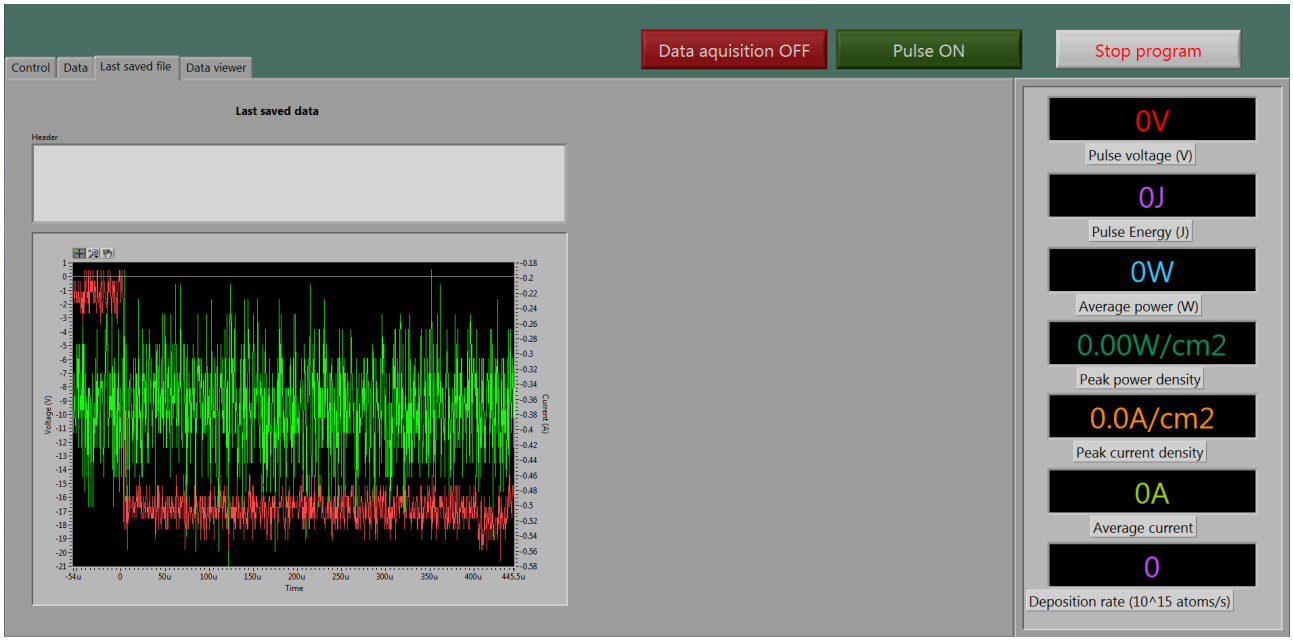

Figure 11: Last saved file interface.

4.3.4 Data viewer tab

The data viewer tab(figure 12) reads multiple files and plots their data simultaneously in the same graph window. There are two graphs, the upper one reads saved waveform files and lower one log files.

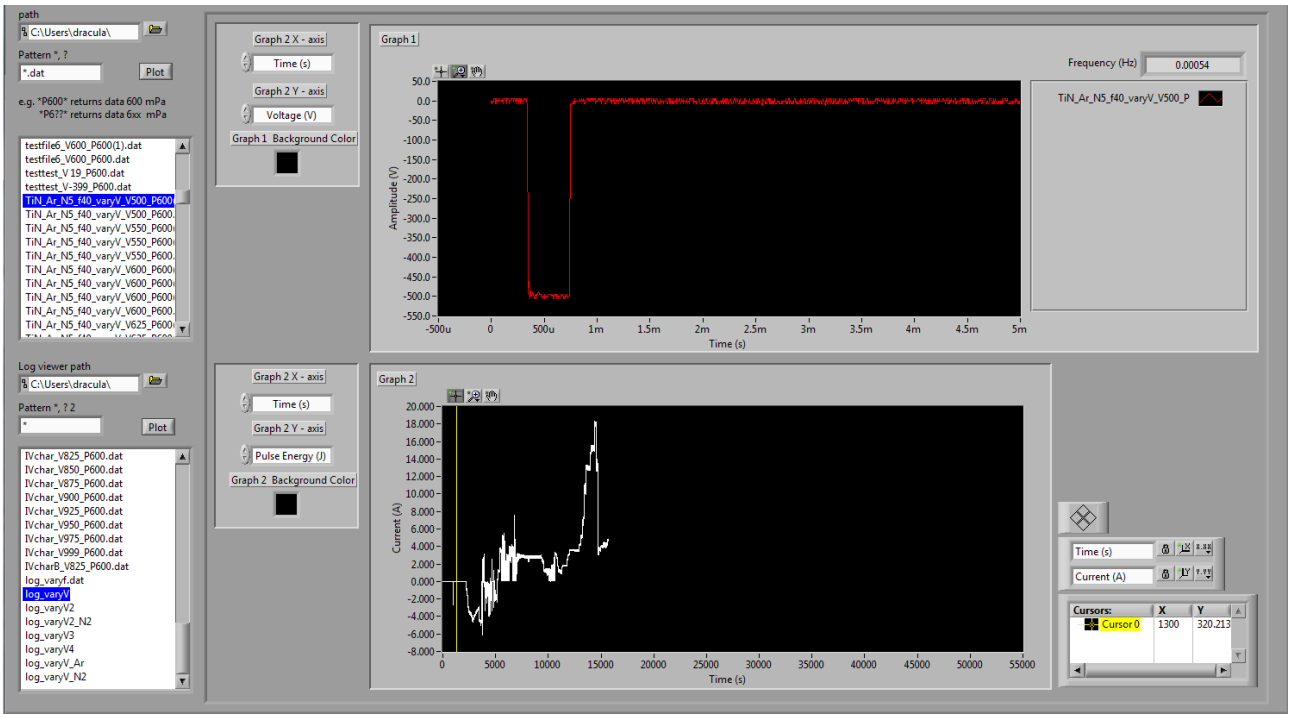

Figure 12: Data viewer interface.

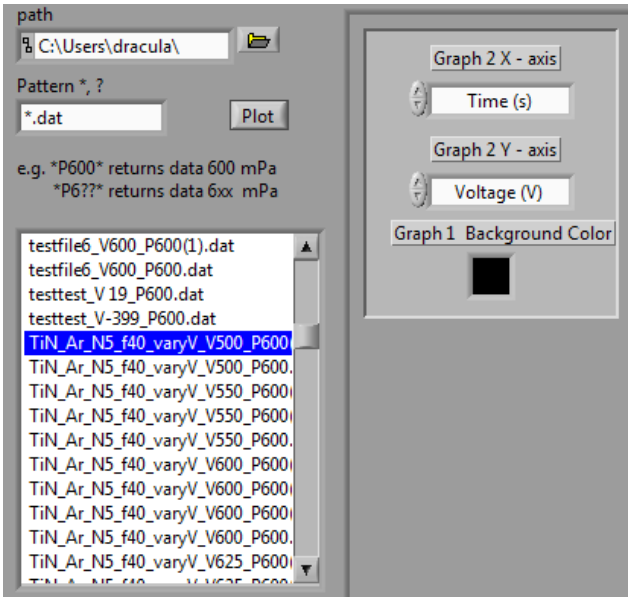

Figure 13: Data viewer file control interface.

Each graph has a *path* and *pattern* (figure 13) option used to locate files. The *pattern* text window is used to filter out specific files in a folder. The user can choose to highlight one or more file names in the file list and data from each highlighted file will be shown.

Both graphs have axis controls so the user can pick which columns should be displayed. Axis names are defined in the files column header. The data viewer is needed to quickly determine the parameters for the next growth process.

4.4 LabView program: Code

One of LabViews strengths is how it handles multiple while loops and parallelism. When you use multiple while loops in LabView it runs them parallel, this simplifies programming quite a bit. It gives the programmer the option to divide the code into modules that can be programmed and tested separately as long as they are independent of data from other modules. In this case the program is divided into five modules (while loops) where each loop has a specific function. The LabView code can be seen in Appendix 1.

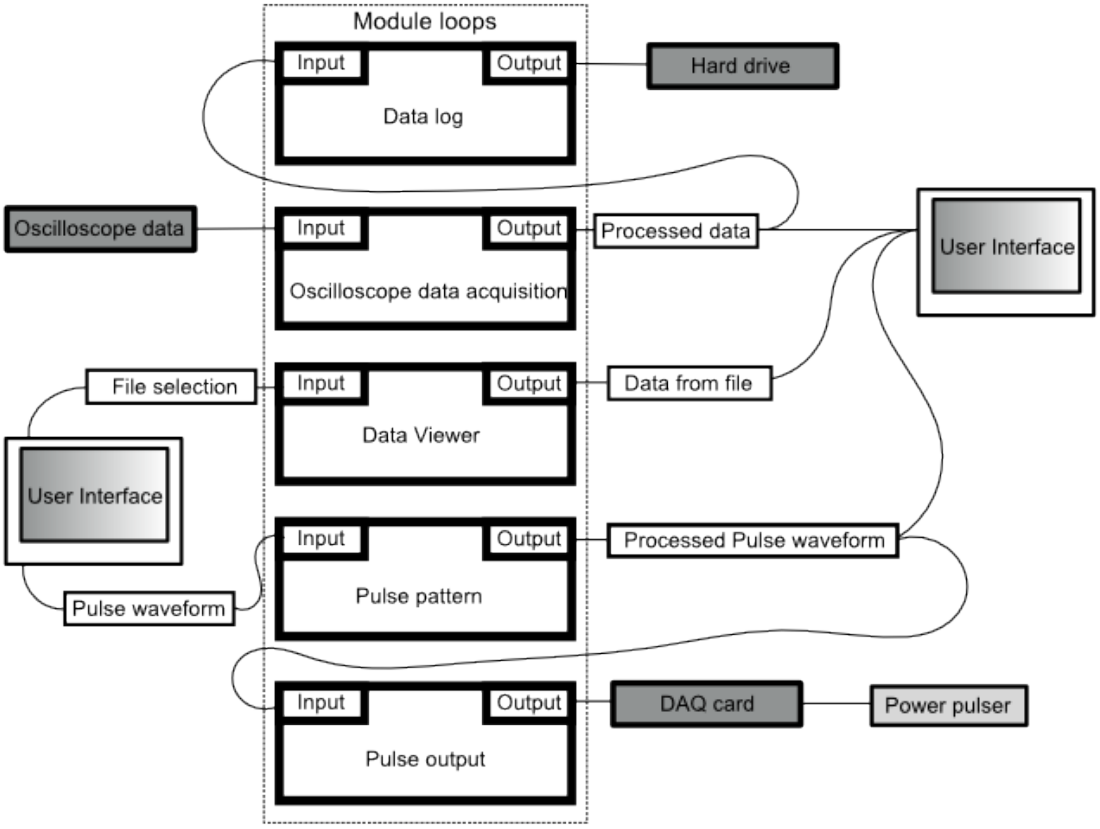

Figure 14: Block diagram code structure. Each box inside the dashed area is a module in a while loop in the code.

4.4.1 Data log loop

Input: Processed data from Oscilloscope data acquisition.

Output: Stores input data in a specific format accommodated for MatLab algorithms used by members of the research group.

The data log loop stores data every second if set to do so, it's limited to store data once per second even though the Oscilloscope data acquisition loop gets data 3 times/s. This is done because there is no need for more data for the time being.

4.4.2 Oscilloscope data acquisition loop

Input: Requests data from Oscilloscope 3 times/s max.

Output: Processed data to Data log loop and user interface.

The oscilloscope data acquisition loop requests data from the oscilloscope and derives the growth process values (average power, peak power density, pulse energy etc). The data is sent to the log loop to be stored and to the user interface where it's displayed in graphs and in the *Latest value* area (see figure 7.).

4.4.3 Data viewer loop

Input: File selection from User Interface.

Output: Data from selected files as graphs.

The Data viewer loop reads data from multiple selected files and presents them in two graphs on the User Interface. It's the only loop that's independent on the rest of the program and could be a stand alone program. Updates every 400ms or if chosen axis is changed.

4.4.4 Pulse pattern loop

Input: Custom pulse waveform from User Interface.

Output: Pulse waveform in correct format for DAQ card. Read by Pulse output loop.

The pulse pattern loop's only function is to quickly make a new pulse waveform if the user changes it in any way on the User Interface. It only runs when changes are detected.

4.4.5 Pulse output loop

Input: Pulse waveform from Pulse pattern loop.

Output: Controls the DAQ card, tells it what pulse to send.

The pulse output loop controls the DAQ card to send continuous pulses. It's partly controlled by the pulse pattern loop, every time the pulse pattern changes the pulse pattern loop signals it has a new pulse waveform causing the pulse output loop to read the new waveform and load it to the DAQ card.

5. Testing and results

Test runs were done frequently to see how the program handles the control of the sputtering process. Future users of the program participated in the tests and changes were made based on their feedback. Many changes were done during testing mostly in what way data is presented.

When the program was deemed stable enough TiN films were grown using HiPIMS and dcMS. Samples were grown at varying output voltage, pulse frequency, temperature and gas pressure. The film crystal structure and grain size was examined by grazing incidence X-ray diffraction (GIXRD) measurements and low-angle X-ray reflectivity (XRR) measurements were performed to determine the film thickness, density and roughness[2]. Samples made using the new program and data gathered from them then became the basis of two articles (articles can be found in Appendix 2), one comparing the difference between samples made using HiPIMS/dcMS and other studying the behavior of HiPIMS vs reactive HiPIMS with N_2 gas as a reactant. Most of the graphs in the first articles are made from data logged by the program and both article use samples grown and measured by the author and F. Magnus during the project time.

By comparing the properties of films made using HiPIMS vs dcMS it could be seen that the HiPIMS process produces highly crystalline films even at room temperature whereas dcMS resulted in films with larger crystallites embedded in amorphous matrix. HiPIMS films are significantly smoother than dcMS grown films, particularly when grown at high temperature[2].

However from studying the effects of reactive HiPIMS it can be concluded that the behavior of the reactive HiPIMS discharge differs significantly from the non-reactive discharge in a somewhat counter intuitive fashion. The current-voltage-time waveforms in a discharge exhibit similar general characteristics as the non-reactive case in that the current rises to a peak due to gas compression, then decays because of rarefaction before rising to a self-sputtering dominated phase[3].

6. Future improvements

There are a few improvements planned for the future.

Implement a way to control the power supply output voltage through the program. If the output voltage can be controlled with the program, it could be possible to control the system during growth to keep some parameters constant through the whole process. This would simplify research by having parameters constant that is not possible at the time.

Add resistance measure equipment for Dracula and improve the resistance measurement setup for Spikes. By replacing the current equipment with equipment that has a higher sample rate it could be possible to measure every pulse sent from the pulser. It is very interesting to see how the film behaves during and after each pulse which to our knowledge is something that has not been done before.

7. Conclusion

All the goals of the project have been met, there is a functioning program capable of controlling the system and grow thin films using HiPIMS. The thin films grown during the project have resulted in two articles with interesting data of the HiPIMS process and are expected to be published in the Journal of Applied Physics and Thin Solid Films. The system will be used to supply various research projects with thin films. For example the institute uses thin films to study the hydrogen uptake of different materials in the search of one suitable to store hydrogen for use as a non volatile power source in future vehicles/devices.

8. References

[1] Milton Ohring. (2002) Materials Science of thin films(2nd ed)

[2] F. Magnus, A.S Ingason, O. B. Sveinsson, S. Olafsson, J. T. Gudmundsson, Comparison of TiN thin films grown on SiO2 by reactive dc magnetron sputtering and high power impulse magnetron sputtering.

[3] F. Magnus, O. B. Sveinsson, S. Olafsson, J. T. Gudmundsson, Current-voltage-time characteristics of the reactive Ar/N2 high power impulse magnetron sputtering discharge.

[4] National Instruements, LabView Help, www.zone.ni.com

Appendix 1

Code overview

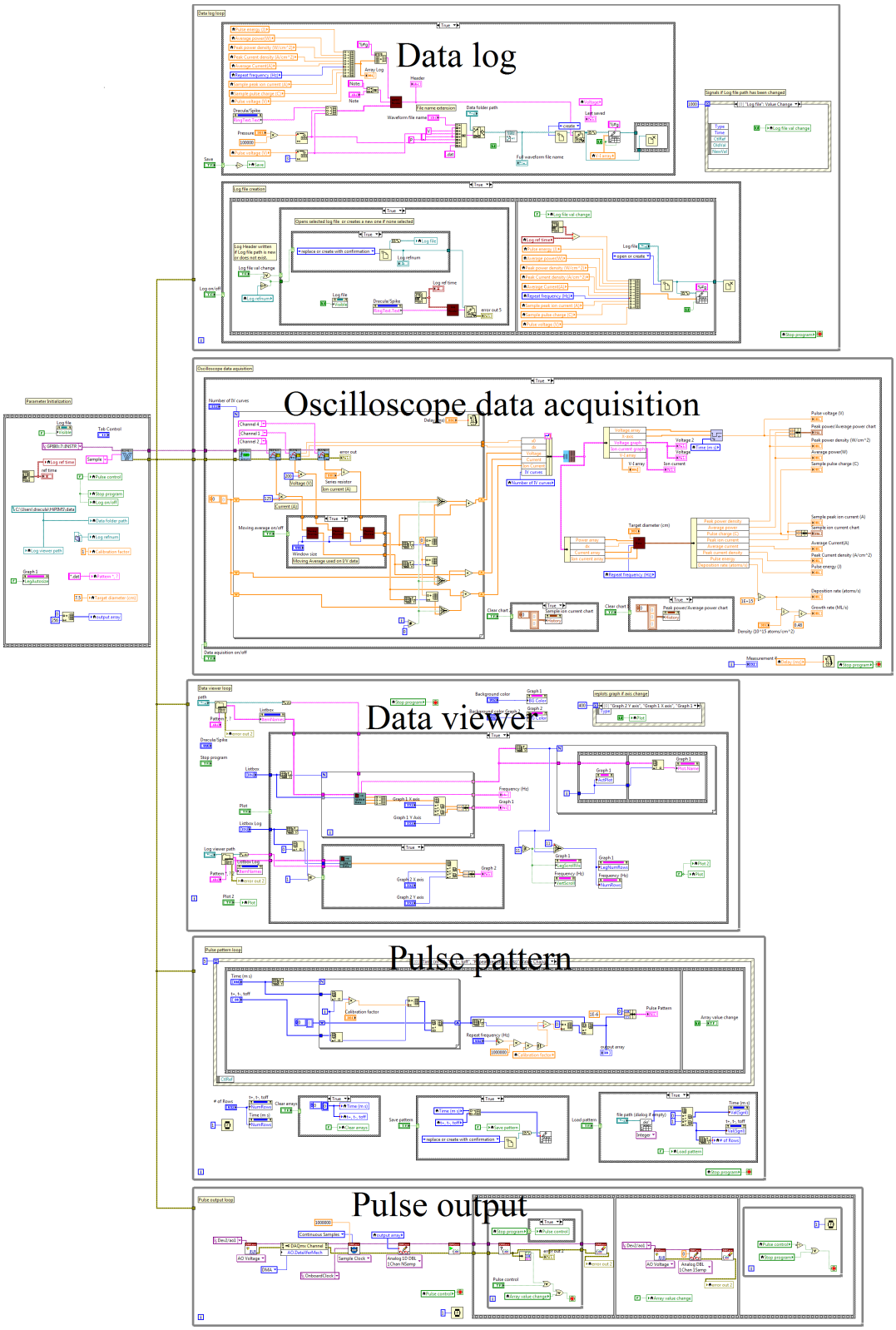

Figure 15: Overview of the LabView program. The program is divided into five loops, Data log, Oscilloscope data acquisition, Data viewer, Pulse pattern and Pulse output.

Data log

The data log loop creates the log file if needed and logs data when the *Save* button is pressed or *Log on/off* button is true.

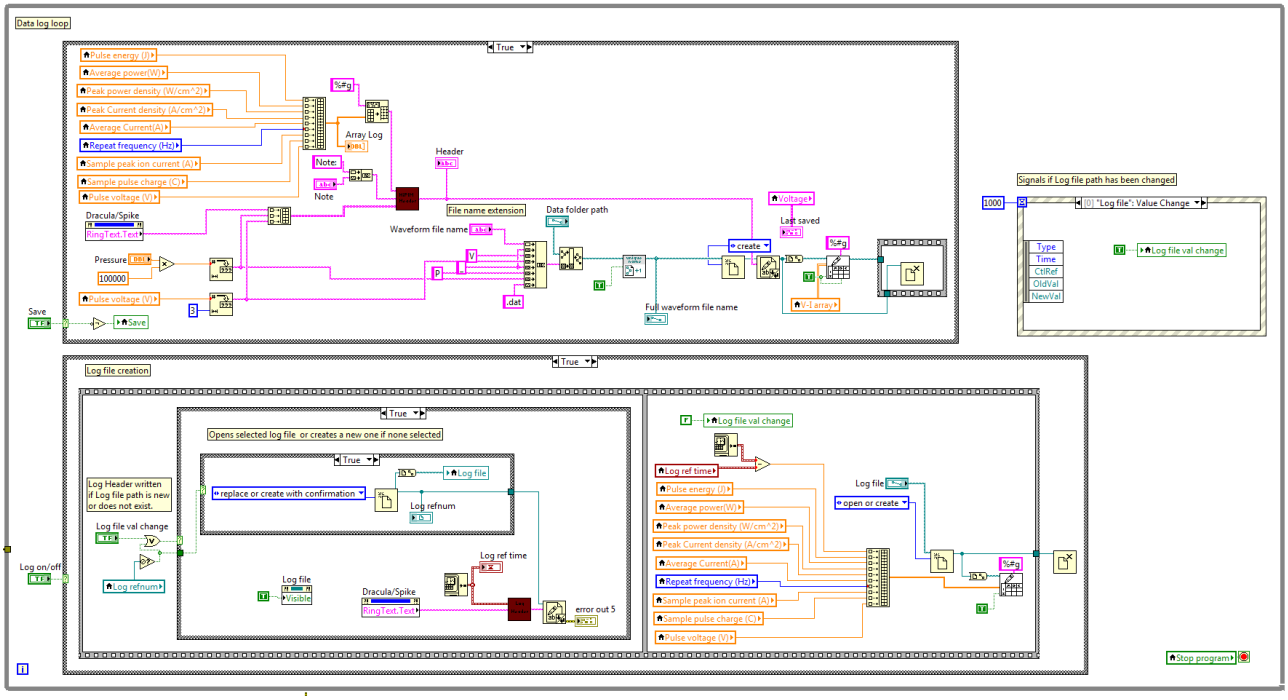

Figure 16: Data log loop code.

Oscilloscope data acquisition

The loop requests data from the oscilloscope every run, due to communication limitations the loop can only run at 3 runs/s. Data is then processed and displayed in Latest value region on the front panel.

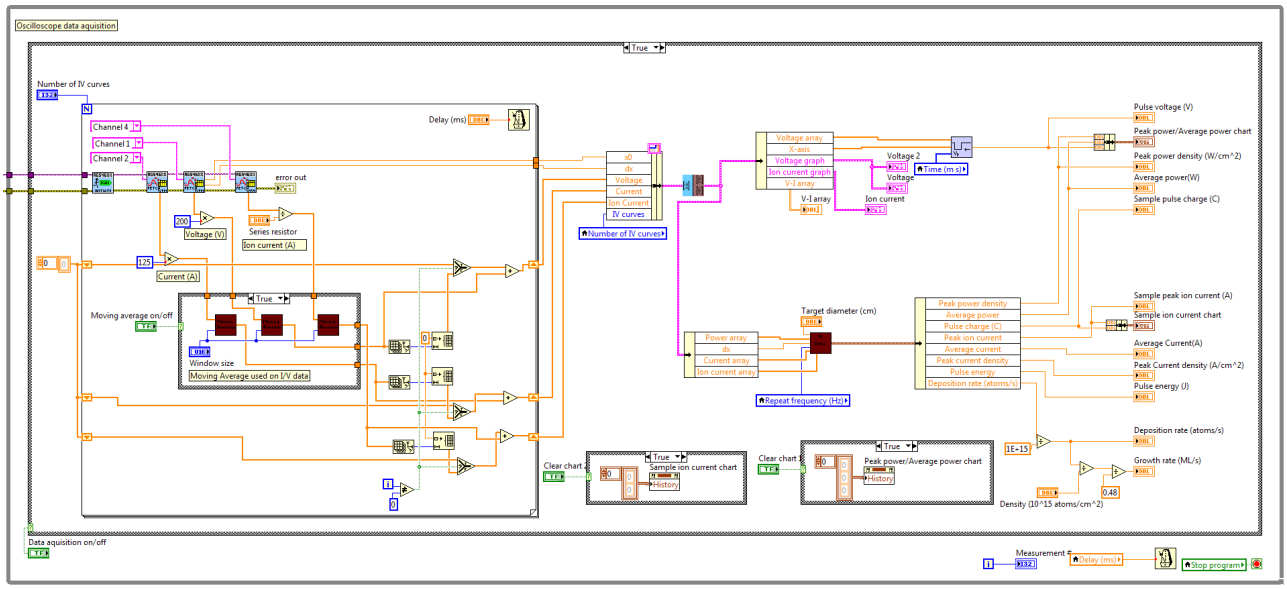

Figure 17: Oscilloscope data acquisition loop.

Data viewer

Reads files and plots their data.

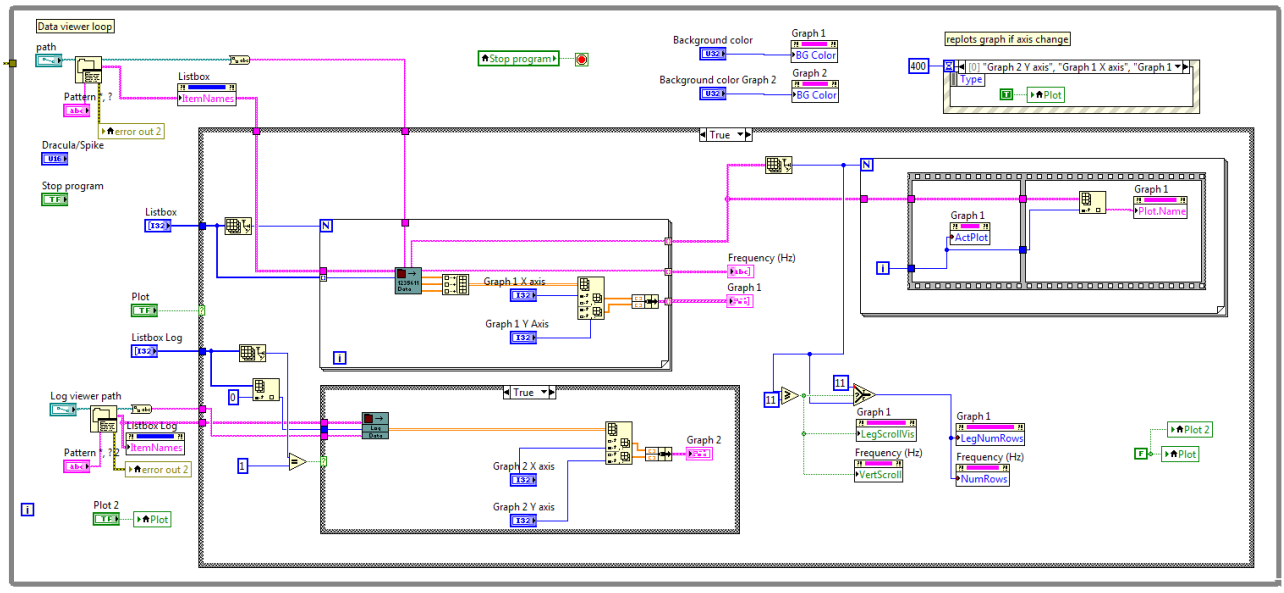

Figure 18: Data viewer loop

Pulse pattern

The pulse pattern is created saved or loaded whenever any of the controls controlling those properties change. The pulse is an array which is read by the pulse output loop.

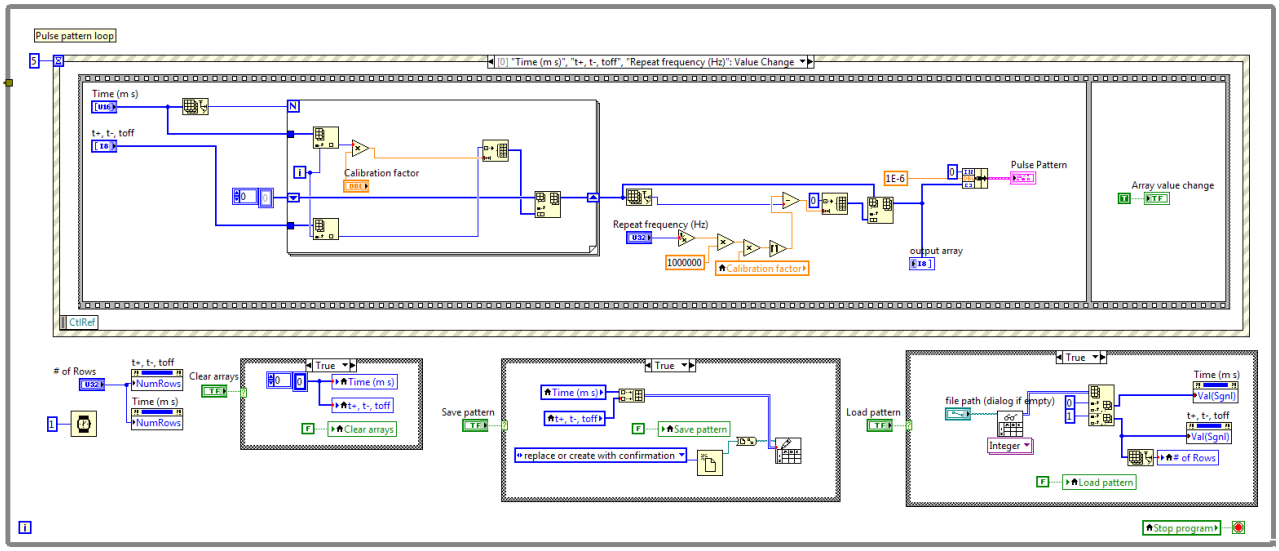

Figure 19: Pulse pattern loop.

Pulse output

The pulse output loop reads the pulse form array every time it runs, resulting in any changes done to the pulse form gets sent to the power supply in the next loop run.

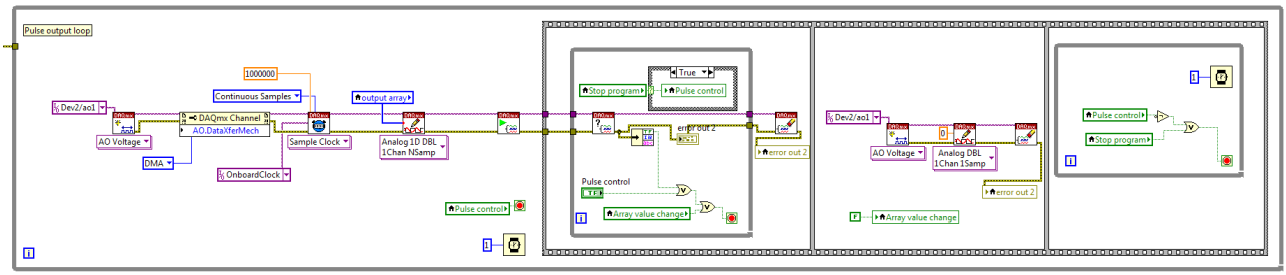

Figure 20: Pulse output loop

Appendix 2

Articles

1. Current-voltage-time characteristics of the reactive Ar/N_2 high power impulse magnetron sputtering discharge.

2. Comparison of TiN thin films grown on SiO2 by reactive dc magnetron sputtering and high power impulse magnetron sputtering.

Current-voltage-time characteristics of the reactive Ar/N_2 high power impulse magnetron sputtering discharge

F. Magnus,[1, a)] O. B. Sveinsson,[1] S. Olafsson,[1] and J. T. Gudmundsson[2]

[1)] *Science Institute, University of Iceland, Dunhaga 3, IS-107 Reykjavik, Iceland*

[2)] *University of Michigan–Shanghai Jiao Tong University Joint Institute, Shanghai Jiao Tong University, 800 Dong Chuan Road, Shanghai 200240, China*

(Dated: 26 August 2011)

The discharge current and voltage waveforms have been measured in a reactive high power impulse magnetron sputtering (HiPIMS) Ar/N_2 discharge with a Ti target for 400 μs long pulses. We observe that the current waveform in the reactive Ar/N_2 HiPIMS discharge is highly dependent on the pulse repetition frequency, unlike the non-reactive Ar discharge. The current is found to increase significantly as the frequency is lowered. This is attributed to an increase in the secondary electron emission yield during the self-sputtering phase, when the nitride forms on the target at low frequencies. In addition, self-sputtering runaway occurs at lower discharge voltages when nitrogen is added to the discharge. This illustrates the crucial role of self-sputtering in the behavior of the reactive HiPIMS discharge.

PACS numbers: 52.80.Vp., 52.25.Jm., 52.40.Hf

[a)]Electronic mail: fridrikm@hi.is

I. INTRODUCTION

The introduction of the planar direct current magnetron sputtering (dcMS) discharge defined the advent of a new era in vacuum coating technology[1]. Magnetron sputtering is widely used to grow thin films of metals, ceramics and oxides for a variety of applications. In a conventional dcMS discharge the majority of ions are the ions of the inert sputtering gas and only a small fraction (∼1%) of the sputtered species is ionized. This is a major drawback of the dcMS process. By pulsing the target to a high power density with unipolar voltage pulses, at a low frequency (a low duty cycle), very high electron densities are achieved[2,3]. The high electron density results in a high ionization fraction of the sputtered vapor. This is referred to as high power impulse magnetron sputtering (HiPIMS) and can be categorized as an ionized physical vapor deposition (IPVD) technique[4,5]. Increased ionization of the sputtered vapor has been demonstrated to improve the quality of the deposited film, such as increasing density[6,7], in particular for substrates of complex shape[8], improving adhesion[9], and improving surface roughness[10]. As an example, TiN thin films grown by reactive sputtering in Ar/N_2 HiPIMS discharges show denser microstructure and smoother surfaces as compared to films grown by conventional dcMS at the same average power[11–14]. It has been argued that the irradiation by Ti^+, N^+ and Ti^{2+} ions provides the desired densification of the films grown by HiPIMS[12].

Most commonly, HiPIMS discharges are operated with short pulses of 50–100 μs and a pulse repetition frequency in the range 50–1000 Hz. These short pulses exhibit a discharge current that rises to a peak and decays again. Anders et al.[15] have explored the current-voltage-time characteristics of an argon discharge for various target materials in detail, using 400 μs pulses. For these longer pulses, the HiPIMS discharge exhibits an initial pressure dependent current peak that is followed by a power and target material dependent second phase. The initial peak is due to strong gas compression and rarefaction and is dominated by the ions of the sputtering gas while the second phase is dominated by self-sputtering of the target material[16]. Anders has also shown that the sustained self-sputtering phase requires the presence of multiply charged ions[17] and indeed titanium ions up to Ti^{4+} have been observed in a HiPIMS discharge[18]. Lundin et al.[19] have observed similar current characteristics when sputtering from a Cr target in an argon discharge for a pulse length of 400 μs. They argue that the depletion of the working gas in front of the target results in a

transition to a dcMS-like high voltage, lower current regime.

During reactive sputtering a reactive gas is added to the inert working gas. This changes the plasma composition by adding new ion species and the target condition can also change due to the formation of a compound on its surface. As a result, the behavior of the discharge is altered significantly as the discharge current (or voltage) is dependent on the ionization energies of the plasma species and the secondary electron emission yield of the target[20]. Here, we study the discharge current waveform in a HiPIMS Ar/N_2 discharge. Using 400 μs long pulses we can observe the time evolution of the pulse, beyond the initial current peak. The effect of varying the discharge voltage and repetition frequency is examined and compared to the non-reactive, pure Ar discharge. In particular, we show that the discharge current becomes highly dependent on the pulse repetition frequency in the reactive discharge.

II. EXPERIMENTAL APPARATUS AND METHOD

The experiment was performed in a custom built cylindrical magnetron sputtering chamber, 29 cm in diameter and 25 cm long[21] with a base pressure of 4×10^{-6} Pa. The sputtering gas was argon of 99.999% purity mixed with nitrogen gas of 99.999% purity. The argon flow rate was $q_{\mathrm{Ar}} = 40$ sccm and the nitrogen flow rate was $q_{\mathrm{N_2}} = 2$ sccm resulting in a total pressure of 0.6 Pa. A circular, balanced, planar magnetron was used, fitted with a Ti target, 75 mm in diameter and of 99.995% purity. The power was supplied by a SPIK1000A pulse unit (Melec GmbH) operating in the unipolar negative mode at constant voltage, which in turn was charged by a dc power supply (ADL GS30). The discharge current and voltage was monitored using a combined current transformer and voltage divider unit (Melec GmbH) and the data were recorded with a digital storage oscilloscope (Agilent 54624A). The pulse repetition frequency and discharge voltage were varied and the pulse length was 400 μs but for high discharge voltages it was necessary to shorten the pulses in order to limit the average power.

The magnetron sputtering chamber is equipped with a sample holder with electrical probes which are held in contact with the substrate by a ceramic shadow mask, as described by Arnalds et al.[21]. By placing a conducting substrate in the sample holder, the ion flux impinging on the substrate can be determined by measuring the current from the substrate to ground I_{f}, as shown in figure 1. The shadow mask determines the size of the ion probe

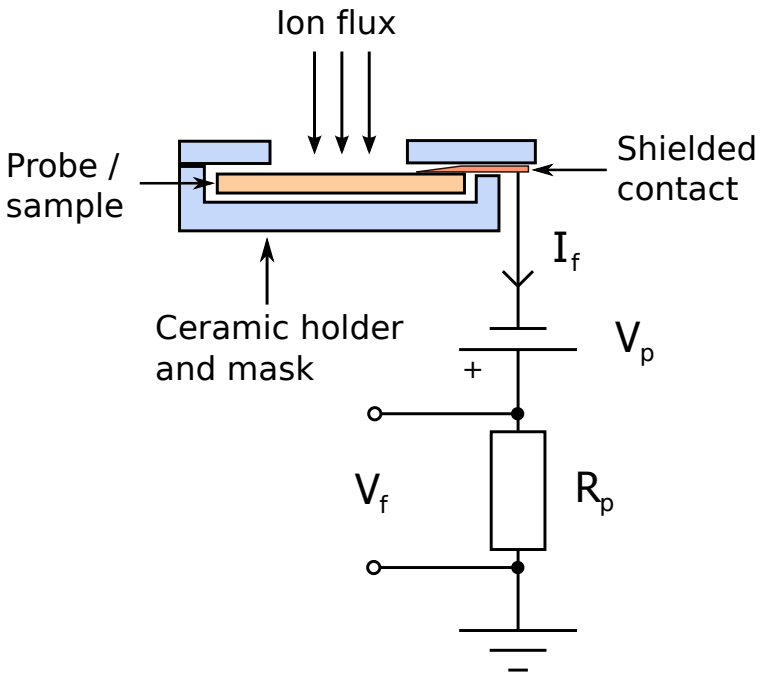

FIG. 1. A schematic of the experimental setup used to measure the ion flux to the substrate.

and also shields the electrical probes from the flux. The current is determined by measuring the voltage drop V_f over the 838 Ω resistor R_p. The ion probe is biased at approximately $-V_\mathrm{p} = -60$ V so that it is firmly in the ion saturation region throughout the duration of the pulse.

III. RESULTS AND DISCUSSION

A. The Ar discharge

The target current waveforms for a pure argon discharge with a titanium target are shown in figure 2 for various discharge voltages. The target voltage pulse (not shown) is initiated at time $t = 0$ and is roughly rectangular. Firstly we note that a delay of a few tens of μs is observed between the target voltage and target current. This delay decreases with increased discharge voltage. It has been seen before that this delay depends on discharge pressure[3] and applied voltage[22] and is determined by the initiation of the discharge as a vacuum breakdown[22]. For voltages up to 600 V the current waveforms can be described by three distinct regions, as previously described by Lundin et al.[19]: (I) plasma initiation

and a current maximum, followed by (II) a decay to a minimum and then (III) a steady state regime that remains as long as the discharge voltage level is maintained. In this low voltage regime we observe that the initial current peak appears earlier in the pulse as the discharge voltage is increased, mainly due to the delay between the voltage pulse and the initiation of the plasma, as discussed above. In addition, the steady-state current level in region (III) is roughly equal to the initial peak value of region (I). Anders et al[15] have shown that the initial peak size is highly dependent on the pressure whereas the current level in region (III) is target material dependent. For discharge voltages higher than 600 V the plateau current increases significantly beyond the value of the peak current and the current waveform becomes unstable. For 750 V and above, a current runaway occurs and therefore we cut the pulse short limit the power dissipation.

The current characteristics seen here are similar to the observations made by Anders et al.[15] The initial peak in current is a result of strong gas compression due to the sudden large flux of atoms from the target. Collisions of the sputtered atoms with the working gas result in heating and expansion of the working gas known as rarefaction. The rarefaction causes the current to fall. As a result, the sputtered atoms replace the working gas atoms in the vicinity of the target to some extent as the pulse evolves. If the plasma density is high enough a significant fraction of the sputtered atoms experience electron impact ionization (the ionization mean free path during the pulse is of the order of 1 cm)[5] and are attracted back to the target to participate in the sputtering process. This is known as self-sputtering and is responsible for the rise in current during the final phase of the pulse.

The sustainability of the self-sputtering process depends on various parameters such as the working gas, the sputter yield, the secondary electron emission yield and the target voltage. Sustainable self-sputtering works only for a limited number of target materials, those that have a high enough sputter yield. Experiments with various materials have revealed that for some materials (including Nb and Ti) the condition set by[23,24]

$$\sigma\beta Y_{\mathrm{SS}} > 1 \tag{1}$$

is fullfilled, where β is the probability of ionization of the sputtered atom, σ is the probability that the newly formed ion returns to the target and Y_{SS} is the self-sputter yield of the ion[15]. Also, an onset of self-sputtering runaway is observed when the applied voltage exceeds a certain value[15]. It has been pointed out by Anders[15,17] that multiply charged metal ions

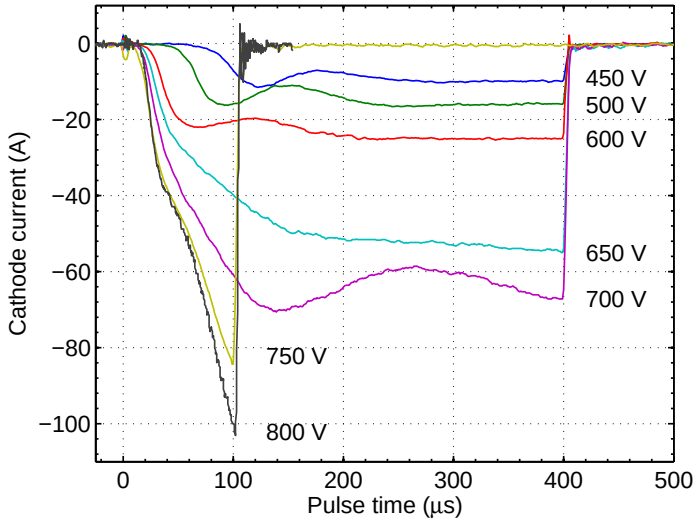

FIG. 2. The discharge current waveform for an argon discharge at 0.6 Pa and pulse repetition frequency of 40 Hz for a range of discharge voltages. For voltages of 750 V and above the pulse length has been reduced to limit the current.

are crucial for the transition of the discharge from argon ion sputtering to self-sputtering, since singly charged metal ions (in the ground state) cannot create the secondary electrons necessary to maintain metal self-sputtering. Thus doubly or higher charged metal ions have to be present in the discharge when it is at the runaway threshold. For some of the common metals like Cu and Ti the ionization energy to create doubly charged ions is relatively low, compared to the ionization energy of argon. Thus the concentration of the doubly charged ions of the sputtered vapor is expected to be high. Indeed, the presence of multiply charged ions is commonly observed in the HiPIMS discharge[12,25,26] including Ti^{4+} ions[18]. Also, Andersson and Anders[27] have demonstrated gasless self-sputtering from a high sputter yield copper target in a HiPIMS discharge where a vacuum-arc discharge was used to initiate the plasma at a background pressure of 10^{-3} Pa. They demonstrate that the magnetron discharge not only self-sustains but amplifies via self-sputtering runaway to high discharge currents. Self-sputtering runaway is driven by a positive feedback. A higher flux of ions leads to increased sputtering, which in turn leads to more neutral atoms that can be ionized in the vicinity of the target and more ions lead to even more sputtering.

The pulse repetition frequency is an important parameter in the HiPIMS processes as it

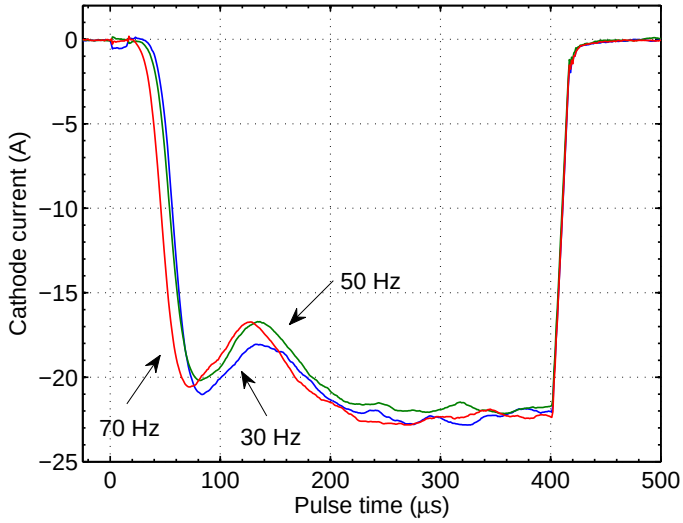

FIG. 3. The discharge current waveforms for an Ar discharge at 0.6 Pa and $V_d = 550$ V for various pulse repetition frequencies.

influences the average power (or current) which in turn affects the deposition rate. A reduced deposition rate compared to dcMS has been one of the concerns raised about the viability of HiPIMS for industrial processes[4,28]. Figure 3 shows the discharge current waveform for an Ar discharge for three pulse frequencies in the range 30–70 Hz. The discharge voltage is kept at a constant value of 550 V. The variation in the current waveforms is minimal in this frequency range although the plasma is initiated slightly earlier in the pulse at the highest frequency. The fact that the current is independent of frequency is useful as it means that the average power can be varied independently of the peak power and without changing the discharge properties.

B. The Ar/N_2 discharge

Let us now examine the effect of introducing a small amount of nitrogen into the discharge. Figure 4 shows the current waveforms for an $Ar/5\%$-N_2 discharge where the discharge voltage is varied. For low voltages the current waveforms are qualitatively similar to the pure Ar case, seen in figure 2. However, the onset of sustained self-sputtering, with a runaway of the current, occurs at a lower voltage than for the Ar discharge. Indeed at 700 V the current rise is so sharp that the pulsing circuitry starts to exhibit oscillations in both voltage and

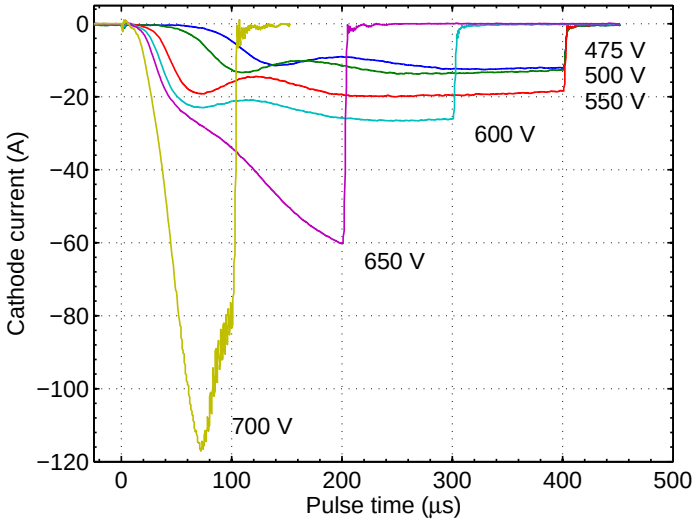

FIG. 4. The discharge current waveform for an Ar/5%-N_2 discharge at a total pressure of 0.6 Pa and pulse repetition frequency of 40 Hz, for a range of discharge voltages. For voltages of 750 V and above the pulse length has been reduced to limit the current.

current known as ringing and this is the reason for the observed drop in current.[29]

The discharge current in an Ar/5%-N_2 discharge for a range of pulse repetition frequencies is shown in figure 5. In stark contrast with the pure Ar discharge, the current is strongly dependent on the repetition frequency in the reactive Ar/N_2 discharge. The discharge current increases substantially with decreasing pulse repetition frequency even though the discharge voltage is kept fixed. Furthermore, the shape of the current changes significantly. At frequencies above 50 Hz the maximum current is reached during the initial peak approximately 100 μs into the pulse. As the frequency is lowered below 50 Hz the current during the latter half of the pulse, i.e. in the self-sputtering regime, outgrows the initial current peak.

The discharge current I_d is the sum of the ion current I_i and the secondary electron current $I_\mathrm{i}\gamma_\mathrm{SE}$ or

$$I_\mathrm{d} = I_\mathrm{i}\,(1 + \gamma_\mathrm{SE}) \tag{2}$$

where γ_SE is the secondary electron emission coefficient of the target material[30]. The ion current is proportional to the ion density n_i which in turn is inversely proportional to the total energy loss per electron-ion pair lost from the system $\mathcal{E}_\mathrm{T}$ i.e.[30]

$$I_\mathrm{i} \propto n_\mathrm{i} \propto \frac{1}{\mathcal{E}_\mathrm{T}}. \tag{3}$$

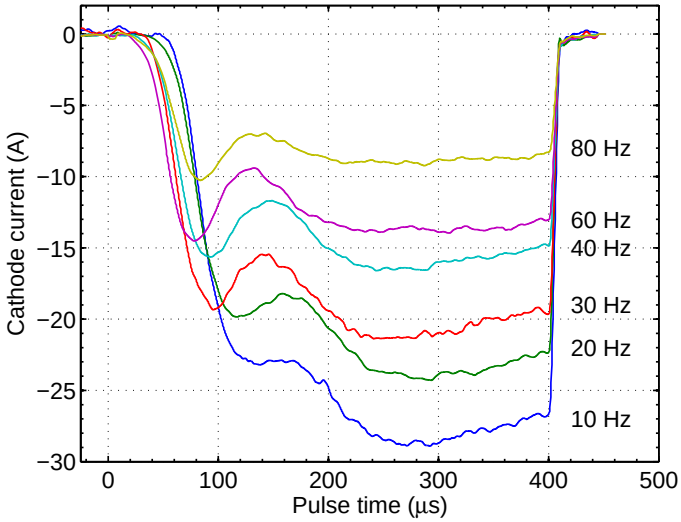

FIG. 5. The discharge voltage and current waveforms for an Ar/5%-N_2 discharge at a total pressure of 0.6 Pa and $V_d = 550$ V for a range of pulse repetition frequencies.

Equations (2) and (3) show that for the discharge current we can write

$$I_d \propto \frac{1}{\mathcal{E}_T}\left(1 + \gamma_{SE}\right). \tag{4}$$

The observed increase in discharge current in the reactive Ar/N_2 discharge can therefore be attributed to: (I) a decrease in $\mathcal{E}_T$ and/or (II) an increase in the secondary electron emission yield of the target. Let us now consider these two cases.

The total energy loss per electron-ion pair lost from the system is composed of three terms

$$\mathcal{E}_T = \mathcal{E}_c + \mathcal{E}_e + \mathcal{E}_i \tag{5}$$

where $\mathcal{E}_c$ is the collisional energy loss per electron-ion pair created and $\mathcal{E}_e$ and $\mathcal{E}_i$ are the kinetic energy loss per electron and ion lost from the system[30]. Both $\mathcal{E}_e$ and $\mathcal{E}_i$ are roughly proportional to and of the order of the electron temperature T_e. $\mathcal{E}_c$ is determined by the composition of ions present in the plasma which in a HiPIMS discharge will evolve during the pulse time. Ehiasarian et al.[26] and Lattemann et al.[12] have shown that the initial phase is dominated by relatively low-energy ions of the working gas (Ar^+, Ar^{2+}, N_2^+, N^+) which is then followed by a phase dominated by the ions of the sputtered species (Ti^+ or Ti^{2+}, N^+). After the pulse has been switched off, thermalized ions of the working gas dominate.

The energy loss per electron-ion pair created, $\mathcal{E}_c$, for N, N_2 and Ar is shown in figure 6 (from ref. 31 and 32). For electron temperatures below 4 V, which is the electron temperature expected for "bulk" electrons in a low-pressure argon dominated discharge, $\mathcal{E}_c$ is high and will be the dominant term in equation (5). In this region, we see that $\mathcal{E}_c$ is similar for both N and N_2 but 1–2 orders of magnitude lower for Ar. This is due to higher electron impact excitation cross sections for N and N_2, and excitation to vibrational levels in N_2. In the energy range expected for secondary electrons ($\sim$100–400 V) the energy loss per electron-ion pair created is slightly lower for N and N_2 than for Ar due to the higher ionization potential for argon. However, in this region $\mathcal{E}_e$ and $\mathcal{E}_i$ are the dominant energy loss terms due to the high electron energy and the difference between $\mathcal{E}_c$ for Ar and N, N_2 is insignificant. Thus the total energy loss is expected to be somewhat higher for an Ar/N_2 mixture than for pure argon. The introduction of nitrogen into the discharge should therefore result in an increase in $\mathcal{E}_T$ and a corresponding decrease in the cathode current.

In the HiPIMS discharge there is a large fraction of Ti ions during the latter part of the pulse. The energy loss per electron-ion pair created for Ti is also shown in figure 6. To calculate $\mathcal{E}_c$ for Ti we use an electron impact ionization cross section from the literature[33,34], assume the excited levels are at 0.81, 0.9, 1.43 and 1.97 eV and each cross section follows the Thomson cross section[30] with a peak at 1/5 of the peak of the ionization cross section. The cross section for electron elastic scattering off of Ti is assumed to be the same as for N[35,36]. We see that the $\mathcal{E}_c$ for titanium is significanly lower than for Ar, N and N_2. So as titanium becomes a significant part of the discharge we expect the discharge current to increase, as is observed in our measurements. Note however, that this applies equally to the reactive and non-reactive discharge and does not explain the differences observed between the two.

As $\mathcal{E}_T$ is expected to increase with the addition of nitrogen we must turn to the secondary electron emission yield to explain the self-sputtering runaway and observed frequency dependence of the current in the reactive discharge. The secondary electron emission yield is governed by the composition of the target (Ti or TiN) and the type of ions that are bombarding it. Studies of dcMS have shown that for a given current the target voltage increases as N_2 is added to the discharge when sputtering from a Ti target[37]. This has been attributed to the increase in $\mathcal{E}_c$ described above but also to the formation of TiN on the target with a slightly lower γ_{SE} than pure Ti[20,38]. According to equation (4) this should result in a decrease in the discharge current. It should be noted that the extent to which

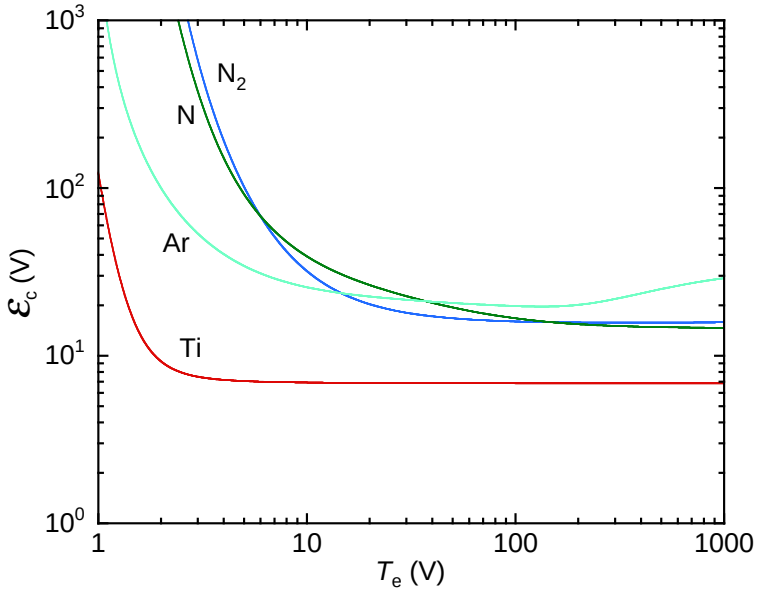

FIG. 6. The collisional energy loss per electron-ion pair created, $\mathcal{E}_c$, as a function of the electron temperature for the ground state nitrogen molecule, $N_2(X^1\Sigma_g^+, v = 0)$, the ground state nitrogen atom, $N(^4S)$, the ground state argon atom, $Ar(^1S_0)$ and the ground state titanium atom, $Ti(^3F_2)$, calculated assuming a Maxwellian electron energy distribution.

the observed increase in voltage is due to changes in $\mathcal{E}_c$ or γ_{SE} is not known.

However, HiPIMS differs significantly from dcMS due to the fact that self-sputtering quickly becomes dominant and the working gas ions (mostly Ar^+ and N_2^+) are depleted from the area in front of the target due to rarefaction. During this self-sputtering phase the plasma ions are supplied by the target and not the working gas. If the target is clean (not poisoned) the self-sputtering consist of Ti ions (mostly singly and doubly charged) impinging on a Ti target whereas if a nitride has formed then Ti ions and N^+ ions are impinging on a TiN target. Anders[17] has pointed out that γ_{SE} is practically zero for singly charged metal ions impacting a target of the same metal. For a potential emission to occur the potential energy (ionization potential) of the projectile has to exceed twice the work function of the target material. A fit to experimentally determined secondary electron emission yield data for various ions on clean surfaces is given as[39,40]

$$\gamma_{SE} = 0.032\,(0.78\mathcal{E}_{iz} - 2\phi) \tag{6}$$

where $\mathcal{E}_{iz}$ is the neutralization energy of the ion and ϕ is the work function of the target

surface. Secondary electron emission can only occur if $0.78\mathcal{E}_{\rm iz} > 2\phi$. The first ionization energies of many metals are insufficient to overcome the workfunction of the target material and therefore multiply charged ions are required. Ti and TiN have workfunctions of 4.3 eV and 3.7 eV, respectively[41]. The first ionization energy of Ti is 6.83 eV so singly charged Ti ions will not be able to sustain self-sputtering for either material whereas Ti^{2+} has an ionization energy of 13.6 eV. On the other hand, the first ionization energy of N is 14.5 eV, so it is clear that $\gamma_{\rm SE}$ will be higher for self sputtering from a TiN target, where N^+ ions are present, than for self-sputtering from a Ti target, where multiply charged Ti ions are needed to create secondary electrons. In a HiPIMS discharge, where self-sputtering is dominant, the discharge current will therefore *increase* when a nitride is formed on the target, opposite to what is seen in the dcMS discharge.

The frequency dependence of the current, seen in figure 5, provides particularly compelling evidence for this effect. At high frequencies a nitride is not able to form between pulses and self-sputtering by Ti ions (singly and multiply charged) from a Ti target is the dominant process. At low frequency the long off-time result in a nitride layer being formed on the target surface and self-sputtering by Ti and N^+ ions from TiN takes place with an increase in secondary electron emission yield and a corresponding increase in discharge current. Indeed, the change in shape of the current waveform points to the self-sputtering process as being responsible for the increase in current.

It is important to know whether the observed changes in the discharge current are reflected in the flux of ions impinging on the substrate. Figure 7 shows the time evolution of the ion flux on the substrate. The ion flux rises steeply shortly after the rise in the cathode current and reaches a maximum at approximately 300 μs into the pulse. This corresponds well with the observed peak in the cathode current. As the the cathode voltage falls to zero the ion flux drops sharply, but interestingly, an ion flux is detected for at least 3.6 ms after the pulse. The peaks at $t_p = 0$ μs and $t_p = 400$ μs are due to noise effects as the pulse voltage rises and falls. Most importantly, the frequency dependence of the ion flux mirrors that of the cathode current i.e. the ion flux increases as the frequency is lowered. The observed increase in secondary electron emission yield with target nitridation should therefore be followed by an increase in deposition rate.

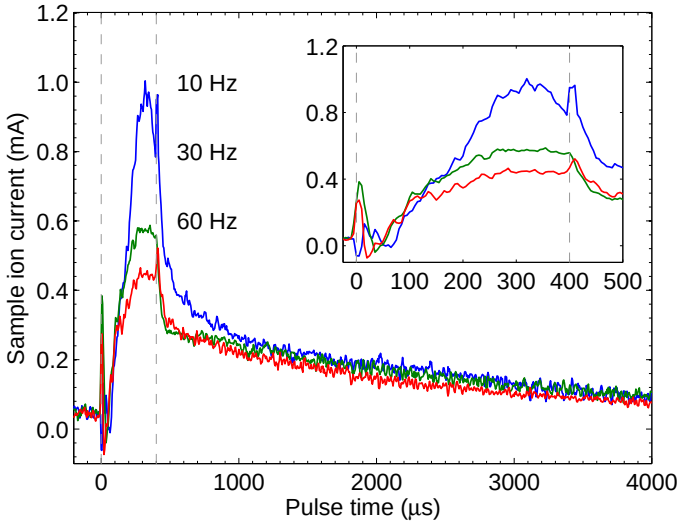

FIG. 7. The time evolution of the ion flux measured at the substrate for the Ar/N_2 discharge driven at three different repetition frequencies. The frequency labels are in the same order as the corresponding ion flux peaks. The duration of the cathode voltage pulse is indicated by the dashed lines. The inset is an enlargement of the pulse on-time. The data have been smoothed with a three-point moving average.

IV. SUMMARY

It can be concluded that the behavior of the reactive HiPIMS discharge differs significantly from the non-reactive discharge in a somewhat counterintuitive fashion. The current-voltage-time waveforms in a discharge exhibit similar general characteristics as the non-reactive case in that the current rises to a peak due to gas compression, then decays because of rarefaction before rising to a self-sputtering dominated phase. However, self-sputtering runaway occurs at lower discharge voltages in the reactive discharge due to the formation of a nitride on the target. The secondary electron emission yield is higher for a nitride target than a titanium target when self-sputtering is the dominant sputtering mechanism. This differentiates HiPIMS from dcMS where self-sputtering is not important. The current rises sharply as the pulse repetition frequency is lowered as a result of increased target nitridation. Measurements show that these increases in self-sputtering result in a similar increase in the ion flux impinging on the substrate.

ACKNOWLEDGMENTS

This work was partially supported by the Icelandic Research Fund grant no 072105003 and the University of Iceland Research Fund.

REFERENCES

[1]J. S. Chapin, Research/Development pp. 37 – 40 (January 1974).

[2]J. T. Gudmundsson, J. Alami, and U. Helmersson, Appl. Phys. Lett. **78**, 3427 (2001).

[3]J. T. Gudmundsson, J. Alami, and U. Helmersson, Surf. Coat. Technol. **161**, 249 (2002).

[4]U. Helmersson, M. Lattemann, J. Bohlmark, A. P. Ehiasarian, and J. T. Gudmundsson, Thin Solid Films **513**, 1 (2006).

[5]J. T. Gudmundsson, Vacuum **84**, 1360 (2010).

[6]J. Alami, K. Sarakinos, F. Uslu, and M. Wuttig, J. Phys. D: Appl. Phys. **42**, 015304 (2009).

[7]M. Samuelsson, D. Lundin, J. Jensen, M. A. Raadu, J. T. Gudmundsson, and U. Helmersson, Surf. Coat. Technol. **202**, 591 (2010).

[8]J. Alami, P. O. A. Petersson, D. Music, J. T. Gudmundsson, J. Bohlmark, and U. Helmersson, J. Vac. Sci. Technol. A **23**, 278 (2005).

[9]A. P. Ehiasarian, J. G. Wen, and I. Petrov, J. Appl. Phys. **101**, 054301 (2007).

[10]K. Sarakinos, J. Alami, and M. Wuttig, J. Phys. D: Appl. Phys. **40**, 2108 (2007).

[11]J. Bohlmark, M. Lattemann, H. Stranning, T. Selinder, J. Carlsson, and U. Helmersson, in *Society of Vacuum Coaters 49th Annual Technical Conference Proceedings* (Society of Vacuum Coaters, Washington DC, USA, 2006), pp. 334–337.

[12]M. Lattemann, U. Helmersson, and J. E. Greene, Thin Solid Films **518**, 5978 (2010).

[13]R. Machunze, A. P. Ehiasarian, F. D. Tichelaar, and G. C. A. M. Janssen, Thin Solid Films **518**, 1561 (2009).

[14]F. Magnus, A. S. Ingason, O. B. Sveinsson, S. Olafsson, and J. T. Gudmundsson, Thin Solid Films , doi: 10.1016/j.tsf.2011.07.041 (2011).

[15]A. Anders, J. Andersson, and A. Ehiasarian, J. Appl. Phys. **102**, 113303 (2007).

[16]D. Horwat and A. Anders, J. Appl. Phys. **108**, 123306 (2010).

[17]A. Anders, Appl. Phys. Lett. **92**, 201501 (2008).

[18]J. Andersson, A. P. Ehiasarian, and A. Anders, Appl. Phys. Lett. **93**, 071504 (2008).

[19]D. Lundin, N. Brenning, D. Jadernas, P. Larsson, E. Wallin, M. Lattemann, M. A. Raadu, and U. Helmersson, Plasma Sources Science and Technology **18**, 045008 (2009).

[20]D. Depla, S. Mahieu, and R. De Gryse, Thin Solid Films **517**, 2825 (2009).

[21]U. B. Arnalds, J. S. Agustsson, A. S. Ingason, A. K. Eriksson, K. B. Gylfason, J. T. Gudmundsson, and S. Olafsson, Rev. Sci. Instrum. **78**, 103901 (2007).

[22]G. Y. Yushkov and A. Anders, IEEE Trans. Plasma Sci. **38**, 3028 (2010).

[23]N. Hosokawa, T. Tsukada, and H. Kitahara, in *Proceedings of the 8th International Vacuum Congress* (Cannes, France, 1980), pp. 11–14.

[24]A. Anders, Surf. Coat. Technol. **204**, 2864 (2010).

[25]J. Bohlmark, M. Lattemann, J. T. Gudmundsson, A. P. Ehiasarian, Y. A. Gonzalvo, N. Brenning, and U. Helmersson, Thin Solid Films **515**, 1522 (2006).

[26]A. P. Ehiasarian, Y. A. Gonzalvo, and T. D. Whitmore, Plasma Processes Polym. **4**, S309 (2007).

[27]J. Andersson and A. Anders, Appl. Phys. Lett. **92**, 221503 (2008).

[28]A. Anders, J. Vac. Sci. Technol. A **28**, 783 (2010).

[29]D. J. Christie, F. Tomasel, W. D. Sproul, and D. C. Carter, J. Vac. Sci. Technol. A **22**, 1415 (2004).

[30]M. A. Lieberman and A. J. Lichtenberg, *Principles of Plasma Discharges and Materials Processing* (John Wiley & Sons, New York, 2005), chap. 10.2 and 14.5, 2nd ed.

[31]E. G. Thorsteinsson and J. T. Gudmundsson, Plasma Sources Sci. Technol. **18**, 045001 (2009).

[32]A. T. Hjartarson, E. G. Thorsteinsson, and J. T. Gudmundsson, Plasma Sources Sci. Technol. **19**, 065008 (2010).

[33]P. L. Bartlett and A. T. Stelbovics, At. Data Nucl. Data Tables **86**, 235 (2004).

[34]H. Deutsch, K. Becker, and T. Märk, Int. J. Mass Spectrom. **271**, 58 (2008).

[35]R. H. Neynaber, L. L. Marinao, E. W. Rothe, and S. M. Trujillo, Phys. Rev. **129**, 2069 (1963).

[36]C. A. Ramsbottom and K. L. Kell, Physica Scripta **50**, 666 (1994).

[37]I. Petrov, F. Adibi, J. E. Greene, W. D. Sproul, and W.-D. Münz, J. Vac. Sci. Technol. A **10**, 3283 (1992).

[38]I. Petrov, L. Hultman, U. Helmersson, J. E. Sundgren, and J. E. Greene, Thin Solid Films **169**, 299 (1989).

[39]R. A. Baragiola, E. V. Alonso, J. Ferron, and A. Oliva-Florio, Surface Science **90**, 240 (1979).

[40]R. A. Baragiola and P. Riccardi, in *Reactive Sputter Deposition*, edited by D. Depla and S. Mahieu (Springer Verlag, Berlin Heidelberg, 2008), pp. 43–60.

[41]B. P. Luther, S. E. Mohney, and T. N. Jackson, Semiconductor Science and Technology **13**, 1322 (1998).

Mater. Res. Soc. Symp. Proc. Vol. 1335 © 2011 Materials Research Society
DOI: 10.1557/opl.2011.1262

Comparison of TiN thin films grown on SiO_2 by reactive dc magnetron sputtering and high power impulse magnetron sputtering

F. Magnus[1], A. S. Ingason[1,2], O. B. Sveinsson[1], S. Olafsson[1], and J. T. Gudmundsson[1,3]

[1]Science Institute, University of Iceland, Dunhaga 3, IS-107, Reykjavik, Iceland
[2]Thin Film Physics, Department of Physics (IFM), Linköping University, Linköping SE-581 83, Sweden
[3]UM-SJTU Joint Institute, Shanghai Jiao Tong University, 800 Dong Chuan Road, Shanghai, 200240, China

ABSTRACT

Thin TiN films were grown on SiO_2 by a reactive dc magnetron sputtering (dcMS) and high power impulse magnetron sputtering (HiPIMS) at range of temperatures from 45 to 600^{o}C and the properties compared. The HiPIMS process produces denser films at lower growth temperature than does dcMS and the surface is much smoother for films grown by the HiPIMS process. The grain sizes of both orientations are smaller in HiPIMS grown films than in dcMS grown films. The [200] crystallites have smaller size than the [111] crystallites for all growth temperatures. For the dcMS process the grain size increases with increased growth temperature for both the [111] and [200] crystallites. For the HiPIMS process the [200] grain size increases monotonically with increased growth temperature, whereas the size of the [111] oriented grains decreases to a minimum for growth temperature of 400 ^{o}C after which it starts to increase with growth temperature.

INTRODUCTION

Thin films of sputter deposited TiN have various applications in microelectronics. Its low bulk electrical resistivity, high chemical stability and high melting point make it well suited as an adhesion layer and diffusion barrier for both aluminum and copper interconnects [1,2]. More recently TiN has been suggested as a potential gate metal in metal-oxide-semiconductor (MOS) devices with high-κ gate dielectrics [3]. All of these applications require fully dense films which can be obtained by increasing the deposition temperature or applying a rather high substrate bias, which is not always desired in the fabrication process.

High power impulse magnetron sputtering (HiPIMS) is a novel ionized physical vapor deposition (IPVD) technique that has received significant interest lately [4,5]. By pulsing the target to a high power density with low frequency, unipolar voltage pulses, with a low duty cycle, a high electron density is achieved which leads to a high ionization fraction of the sputtered vapor. TiN thin films grown on silicon by reactive HiPIMS show denser microstructure and smoother surfaces as compared to films grown by conventional dc magnetron sputtering at the same average power [6,7]. Lattemann et al. [7] have also reported on fully dense, smooth surface, non-faceted (111)-textured TiN films grown by HiPIMS at ambient temperature without a substrate heater or substrate bias.

Here we compare the morphology of TiN thin films grown by dc magnetron sputtering (dcMS) and HiPIMS on thermally oxidized Si (100) substrates. The film crystal structure and grain size was examined *ex-situ* by grazing incidence X-ray diffraction (GIXRD) measurements

and low-angle X-ray reflectivity (XRR) measurements were performed to determine the film thickness, density and roughness.

EXPERIMENT

TiN thin films were grown in a custom built magnetron sputtering chamber [8] with a base pressure of 4 x 10^{-6} Pa. The sputtering gas was argon of 99.999 % purity mixed with nitrogen gas of 99.999 % purity. The argon flow rate was q_{Ar} = 40 sccm and the nitrogen flow rate q_{N2} = 2 sccm and a throttle valve was used to set a total growth pressure of 0.7 Pa. A Ti target, 75 mm in diameter and of 99.995 % purity, was used. The substrates were thermally oxidized Si(001) with an oxide thickness of 500 nm. The substrate temperature was controlled during growth with a 1.5 inch circular plate heater, separated from the substrate holder by a 2 mm gap [8].

Film deposition was carried out by both dcMS and HiPIMS. The dcMS was performed at 100 W applied power but the details of the dcMS process are described elsewhere [9]. For HiPIMS the power was supplied by a SPIK1000A pulse unit (Melec GmbH) operating in the unipolar negative mode at constant voltage, which in turn was charged by a dc power supply (ADL GS30) [10]. The discharge current and voltage was monitored using a combined current transformer and a voltage divider unit (Melec GmbH) and the data were recorded with a digital storage oscilloscope (Agilent 54624A). The cathode voltage was varied in the range 630-650V in an attempt to achieve a similar peak power density for all samples [10]. The pulse length was 150 μs and the pulse repetition frequency was 75 Hz. The peak power density was 0.65 ± 0.10 kW/cm^2 and the power averaged over one period was 160 ± 15 W. The growth time is 30 minutes for dcMS process and 53 minutes for HiPIMS process.

X-ray diffractometry (XRD) was carried out using a PANalytical X'pert diffractometer (Cu K_a, wavelength 0.15406 nm) mounted with a hybrid monochromator/mirror on the incident side and a 0.27° collimator on the diffracted side. A line focus was used with a beam width of approximately 1 mm. The grazing incidence (GI) XRD scans were carried out with the incident beam at $\theta < 1°$. The film thickness and density was determined by low-angle X-ray reflectivity (XRR) measurements with an angular resolution of 0.005°. The low incident angle means that these measurements probe almost the entire film area.

RESULTS AND DISCUSSION

All the films, grown by both dcMS and HiPIMS, are polycrystalline as determined by the presence of peaks in GIXRD scans. A comparison of GIXRD scans for HiPIMS and dcMS-grown films at 200 °C and 600 °C can be seen in Figure 1. For films grown by HiPIMS, the [111], [200] and [110] peaks are observed at all growth temperatures. In films grown by dcMS, there are no clear TiN peaks in the scan of the room-temperature-grown film and only the [111] orientation is observed in the film grown at 100 °C. For growth temperatures from 200 °C and upwards, all three peaks are observed in the dcMS-grown films as well. The grain size of the differently oriented crystallites can be deduced from the full width at half-maximum of the corresponding peaks, using the Scherrer formula. The grain size of the [111] and [200] crystallites is plotted in Figure 2 for the range of growth temperatures. The grain size is normalized by the film thickness due to the difference in thickness of the films grown by the two methods. We can see that at low temperatures, the HiPIMS films grow preferentially in the [111]

orientation and the [111] grain size is larger than that of the dcMS films. The grain size increases with temperature and by 200 °C the grain size in the dcMS films overtakes that of the HiPIMS films. Interestingly, despite the larger grains in the high-temperature-grown dcMS films, there is still a much larger amorphous contribution. We can therefore draw the conclusion that dcMS films consist of large crystallites in an amorphous matrix whereas HiPIMS process results in pure nanocrystalline films, regardless of growth temperature. This is consistent with other reports of HiPIMS of transition metal nitrides where a transition from polycrystalline to nanocrystalline films has been observed when the metal ion flux increases. The intense ion irradiation during HiPIMS induces an apparent periodical disruption of the individual grain growth [11,12].

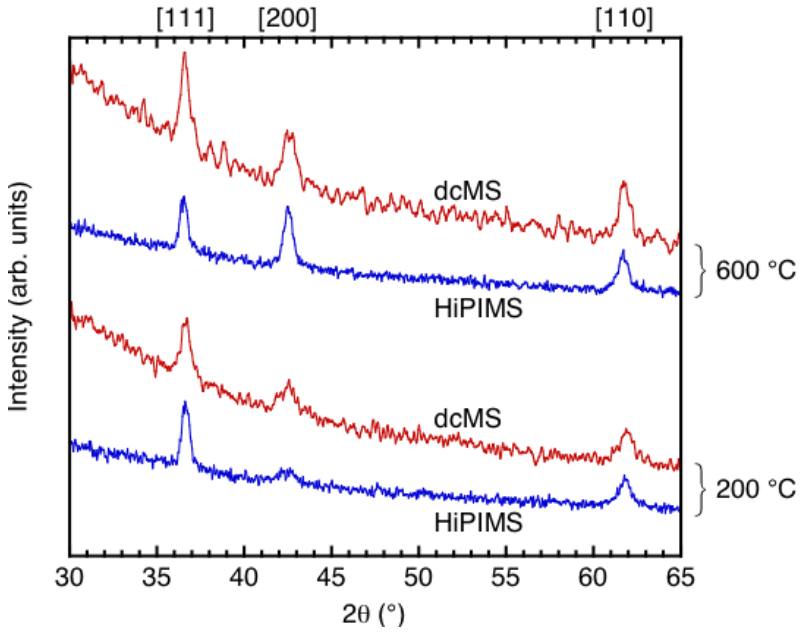

Figure 1. Grazing incidence X-ray diffraction scans of dcMS and HiPIMS-grown TiN films. The growth temperature is shown on the right and the peaks are labeled on top. The curves are shifted for clarity.

A comparison of the XRR from films grown by the two methods is shown in Figure 3. The film density is related to the critical angle at which the reflected intensity starts to drop rapidly. Despite the differences in crystallinity, the density is similar over the entire temperature range. The most significant difference observed by the XRR measurements is the difference in surface roughness. The surface roughness influences the drop in reflected intensity with increasing 2θ as well as the suppression of the interference fringes. Clearly, the film grown by HiPIMS at 600 °C is much smoother than the corresponding dcMS film. The smoothening of film surfaces during HiPIMS has also been attributed to energetic ion bombardment [13].

The density, film thickness and surface/interface roughness can be quantified by fitting the XRR data using the Parrat formalism. Two layers of different densities are required to model the scans of the films grown at 200 °C whereas a single layer model suffices to describe the data for the films grown at 600 °C. Indeed the rms surface roughness turns out to be 1.3 nm and 3.2 nm for the films grown at 600 °C by HiPIMS and dcMS, respectively. It should also be noted when comparing these roughness values that the HiPIMS film is approximately 15% thicker than the dcMS film so the difference is underestimated due to the effect of statistical roughening [14].

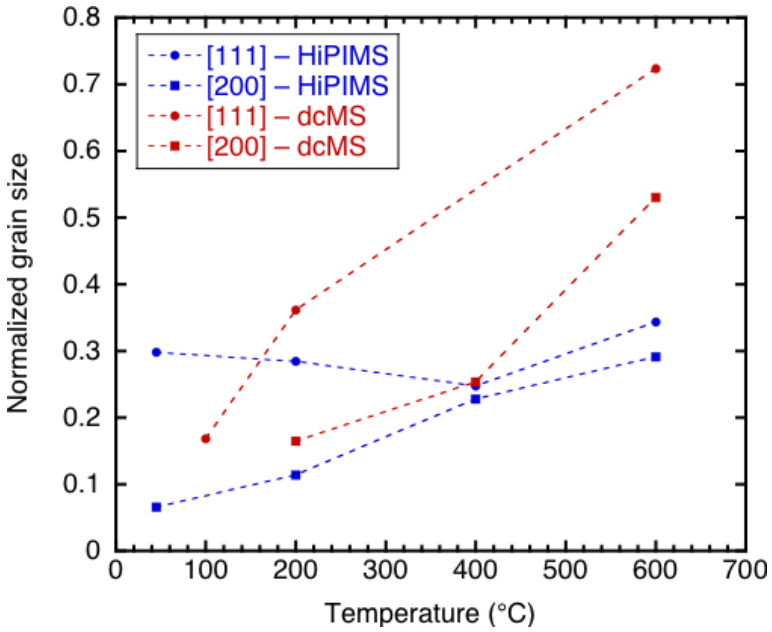

Figure 2. The grain size of [111] and [200] crystallites in both HiPIMS and dcMS-grown films, versus the growth temperature. The grain size is normalized by the film thickness. Where data are missing, no [111] or [200] peaks were observed.

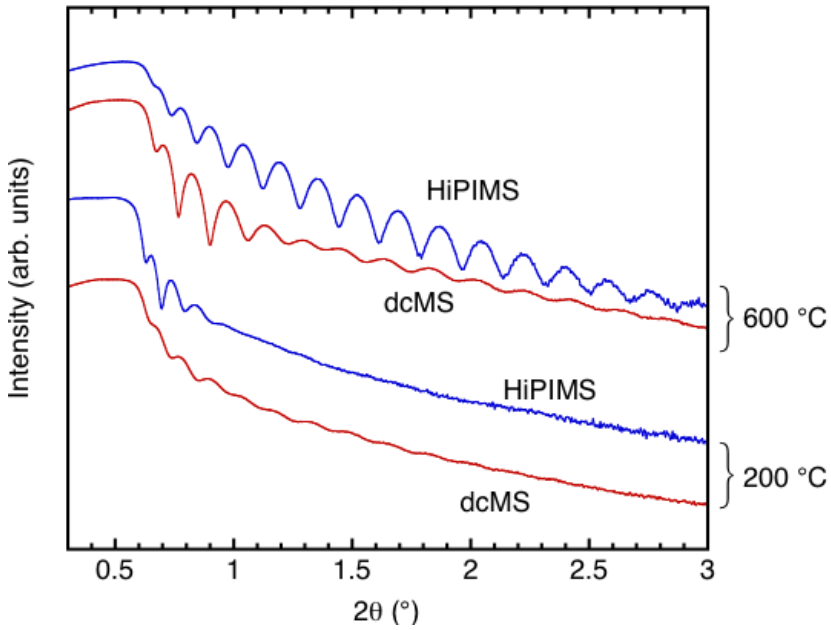

Figure 3. XRR scans of films grown by HiPIMS and dcMS at the growth temperature shown on the right. The curves have been shifted for ease of comparison.

CONCLUSIONS

Thin TiN films were grown on SiO_2 at growth temperatures ranging from room temperature to 600 °C by dcMS and HiPIMS. The HiPIMS process produces highly crystalline films even at room temperature whereas dcMS results in films with larger crystallites embedded

in amorphous matrix. HiPIMS films are significantly smoother than dcMS grown films, particularly when grown at high temperature.

ACKNOWLEDGMENTS

This work was partially supported by the University of Iceland Research Fund and the Icelandic Research Fund grant no 072105003.

REFERENCES

1. G. Gagnon, J. F. Currie, J. L. Brebner, and T. Darwall, J. Appl. Phys. **79** 7612 (1996)
2. G. S. Chen, J. J. Guo, C. K. Lin, C.-S. Hsu, L. C. Yang, and J. S. Fang, J. Vac. Sci. Technol. A **20** 479 (2002)
3. R. Chau, S. Datta, M. Doczy, B. Doyle, J. Kavalieros, M. Metz, IEEE Electron Device Letters **25** 408 (2004)
4. U. Helmersson, M. Lattemann, J. Bohlmark, A. P. Ehiasarian, J. T. Gudmundsson, Thin Solid Films **513** 1 (2006)
5. J. T. Gudmundsson, Vacuum **84** 1360 (2010)
6. J. Bohlmark, M. Lattemann, H. Stranning, T. Selinder, J. Carlsson, and U. Helmersson, Society of Vacuum Coaters 49th Annual Technical Conference Proceedings, Washington DC, 2006, pp. 334–337.
7. M. Lattemann, U. Helmersson, and J. E. Greene, Thin Solid Films **518** 5978 (2010)
8. U. B. Arnalds, J. S. Agustsson, A. S. Ingason, A. K. Eriksson, K. B. Gylfason, J. T. Gudmundsson, and S. Olafsson, Rev. Sci. Instrum. **78** 103901 (2007)
9. A. S. Ingason, F. Magnus, J. S. Agustsson, S. Olafsson, J. T. Gudmundsson, Thin Solid Films **517** 6731 (2009)
10. F. Magnus, A. S. Ingason, O. B. Sveinsson, S. Olafsson, J. T. Gudmundsson, Thin Solid Films, submitted 2011
11. J. Alami, K. Sarakinos, F. Uslu and M. Wuttig, J. Phys. D: Appl. Phys. **42** 015304 (2009).
12. I. Petrov, P. B. Barna, L. Hultman and J. E. Greene, J. Vac. Sci. Technol. A **21** S117 (2003).
13. J. Alami, P. O. A. Persson, D. Music, J. T. Gudmundsson, J. Bohmark and U. Helmersson, J. Vac. Sci. Technol. A **23** 278 (2005).
14. D. L. Smith, *Thin-Film Deposition: Principles and Practice*. (McGraw-Hill, Boston, Massachusetts, 1995).